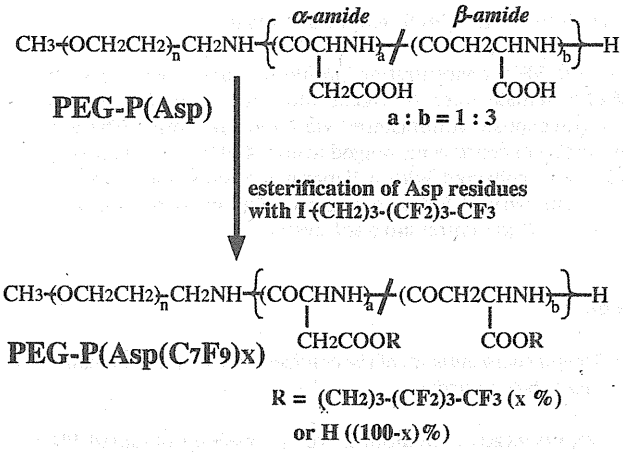

Fig. 2. Synthesis of the fluorocarbon-containing block copolymer PEG-P(Asp(C7F9)x).

2.00 mol. equivalents to the Asp residue, I-(CH2)3-(CF2)3-CF3 in Fig. 2) and 0.972 g of 1,8-diazabicyclo[5.4.0]undec-7-ene (DBU, which is 1.01 mol. equivalents to the Asp residue). DBU is a very strong base, and can induce ionization in a carboxyl group of the aspartic acid residue in an organic solvent, DMF. The reaction mixture was heated at 50 °C for 16 h. An ester formed at the Asp residue through a nucleophilic substitution reaction of the ionized carboxyl group with I-(CH2)3-(CF2)3-CF3. After this 16-h reaction, the reaction mixture was poured into 200 mL of ice-cold diethyl ether for precipitation of the polymer. The precipitated polymer was filtered and washed with diethyl ether. The obtained polymer was dissolved in 20 mL of DMSO, to which was added 2.11 mL of 6 N hydrochloric acid. This acid works for removal of DBU from polymers. This polymer solution was dialyzed with a Spectra/Por 6 dialysis membrane (molecular weight cut-off is 1000) against DMSO for 2 days and against milliQ water for an additional 2 days, followed by freeze-drying. Yield was 2.436 g. To determine the contents of the fluorinated ester group of the polymer, we used ^{1}H NMR spectroscopy in DMSO-d_6 containing 3 v/v% trifluoroacetic acid. For this determination, we identified a peak area ratio between the methylene protons ($-COOCH_2\underline{CH_2}CH_2CF_2CF_2CF_2CF_3$) at 1.8 ppm of the ester group and the methylene protons ($-OC\underline{H_2}\underline{CH_2}-$) at 3.6 ppm of the PEG block. The esterification percentage (x in Fig. 2) was revealed to be 59%. The other compositions of block copolymers were synthesized according to the same method with various molar ratios of I-(CH2)3-(CF2)3-CF3 and DBU with respect to the aspartic acid residue. Table 1 lists all the compositions of the synthesized block copolymers.

Table 1
Compositions of PEG-P(Asp(C7F9)x).

Code	M.W. of PEG	Asp unit number (n)	Esterification degree (x%)
F-6%	5200	22.1	5.9
F-15%	5200	23.3	14.6
F-39%	5200	22.1	38.5
F-59%	5200	26.0	58.5
F-67%	5200	22.1	67.0

2.3. Preparation of PFC-containing nano-emulsions

We examined preparations of PFC5-containing nano-emulsions according to two methods using a high-pressure emulsifier and a bath-type sonicator.

2.3.1. Preparation with a high-pressure emulsifier

We dissolved PEG-P(Asp(C7F9)15) block copolymer by stirring it in distilled water at a concentration of 4.0 wt. % of the solution, and added perfluoropentane (PFC5) and perfluorohexane (PFC6) at each 1.25 vol.% of the solution. We vigorously stirred the solution with a homogenizer Polytron (Kinematica AG, Tokyo, Japan) at 25,000 rpm for 10 s. Then, we conducted emulsification using a high-pressure emulsifier EmulsiFlex-C5 CSC (AVESTIN, Inc., Ottawa, Ontario, Canada) at 4 °C for 6 min at ca. 50 MPa. We collected a white emulsion, and filtered it with a Sartorius Minisart (R) filter (1.2 μm pore, Sartorius AG, Göttingen, Germany).

2.3.2. Preparation with a bath-type sonicator

We dissolved PEG-P(Asp(C7F9)x) block copolymers in MilliQ water at a concentration of 1.0 to 4.0 wt.% of water. In case of a high ester content such as x = 59, we heated (up to ca. 40 °C) and sonicated the solutions until we obtained a transparent polymer solution. The polymer solution was transferred to a 1.5-mL glass vial that was sealed with a Teflon–silicon rubber cap (Chromacol auto-sampler vial 2-SV for HPLC; GL Science, Inc., Tokyo, Japan), and was cooled on ice. Then, we added perfluoropentane (PFC5) and perfluorohexane (PFC6) at 0.5–4.0 vol.% of water. We confirmed PFCs' position at the bottom of the solution. (Sometimes PFCs, whose densities are much greater than water's, did not go into the aqueous solution. Therefore, we shook the vial vigorously to allow PFC droplets to sink to the bottom by force of gravity.) Then, we sealed the vial with a cap, and applied sonication for 3 min with a bath-type sonicator Branson model 1510 (oscillating frequency at 42 kHz, max. power intensity: 90 W, Danbury, CT, USA). The temperature of the bath was kept constant with degassed cold and hot water. In all the sonication procedures, we had a constant water level in a sonicator bath and a fixed position of the vial in order to obtain sonication conditions that were as identical to one another as possible. Finally, we collected a supernatant by leaving unincorporated PFC droplets at the bottom.

Table 2
Effects of polymer composition and sample volume on PFC5 incorporation behaviors.

Run	Polymer	Sample volume (μL)	PFC5 concentration (vol.%)[a]	Cumulant average diameter (nm)[a]
1	F-6%	300	0.840 ± 0.097	261.2 ± 3.4
2	F-15%	300	0.948 ± 0.131	232.4 ± 14.5
3	F-39%	300	0.625 ± 0.074	198.4 ± 33.3
4	F-59%	300	0.669[b]	133.9[b]
5	F-67%	300	0.682 ± 0.060	222.8 ± 37.9
6	F-59%	300	0.682 ± 0.074	205.5 ± 15.8
7	F-59%	300	0.634 ± 0.361	173.5 ± 24.5
8	F-59%	700	1.110[b]	231.8[b]
9	F-59%	1200	1.792[b]	280.6[b]

[a] Average ± standard deviation (n = 3) except runs 4, 8, and 9.
[b] Average of two preparations.

In order to measure amounts of the polymer chains that were not included in the PFC-emulsions, we carried out the following experiment. PFC-emulsion was prepared in the conditions of Run 4 of Table 2; polymer: F-59%, sample volume: 300 μL, polymer concentration: 4 wt.%, PFC5: 2 vol.%, PFC6: 2 vol.%, sonication at 40 °C for 3 min. The obtained emulsion was transferred into a 1.5 mL Eppendorf-type poly(propylene) tube and centrifuged at 13,200 rpm for 5 min with an Eppendorf centrifuge model 5415D (Eppendorf Co., Ltd. Japan, Tokyo, Japan). The emulsion was found to precipitate at the bottom. 200 μL of the supernatant was collected and freeze-dried. We calculated the polymer amounts that were not included in the PFC-emulsions by multiplying 1.5 (=300 μL/200 μL) to the freeze-dried polymer weight. As a control, we carried out the same experiment just only for the polymer (without addition of TFC5 nor TFC6).

2.4. Measurements

2.4.1. Dynamic light scattering (DLS)

The size of emulsions was measured with a dynamic light scattering (DLS) instrument, the DLS-7000 (Otsuka Electronics, Tokyo, Japan). DLS samples were prepared through appropriate dilution of the emulsions with commercial distilled water for internal injection (Otsuka Pharmaceutical Co. Ltd., Tokyo, Japan). The measurements were made at 25 °C, and scattering was observed at a 90° angle with respect to the incident beam. The cumulant average particle size and the particle size distribution from a non-negative least square method were determined by the use of software provided with the instrument.

2.4.2. Gas chromatography

We measured concentrations of PFC5 using two gas chromatograph systems as described below. In both cases, we successfully obtained clear separation of PFC5's peak from PFC6's peak, and carried out quantitative analyses using a standard sample of PFC5. Therefore, the two gas chromatograph systems gave us identical results. However, we only used the (2) system described below for blood samples because its pre-heating function was essential for measurements of blood samples.

2.4.2.1. Gas chromatograph system. We measured PFC5 using a gas chromatograph model G-6000 (Hitachi High-Technologies Corporation, Tokyo, Japan) equipped with a Gaskuropack 54 80/100 packed column (GL Sciences, Inc., Tokyo, Japan) and an FID detector at 200 °C. Carrier gas was nitrogen at a flow rate of 300 mL/min. 5 μL of a sample solution were injected into the gas chromatograph system with a micro syringe at 0 min. Column temperature was controlled in the following manner; 100 °C (0 min), raised at a rate of 5 °C/min until 130 °C (6 min), and then raised at a rate of 60 °C/min until 190 °C (7 min), followed by maintenance of 190 °C for 2 min. PFC5 and PFC6 were found to elute at 3.8 min and 6.4 min, respectively.

2.4.2.2. Gas chromatograph system. We measured PFC5 using a gas chromatograph system GC-2014 (Shimadzu Corp., Kyoto, Japan) equipped with an FID detector at 250 °C. We used two tandem-connected two columns: DB-WAX 127-7012 (Agilent Technologies Japan, Ltd., Tokyo, Japan) and RESTEK Rt-QBond 19741 (Shimadzu GLC Ltd., Tokyo, Japan). Carrier gas was helium at a flow rate of 20 mL/min. Either 100 or 544 μL of a sample solution were heated at 200 °C and injected with a headspace autosampler TurboMatrix Trap 40 (PerkinElmer Japan Co., Ltd., Yokohama, Japan). Column temperature was constant at 150 °C. PFC5 and PFC6 were found to elute at 3.6 min and 4.4 min, respectively.

2.5. Measurements of PFC5 concentration in blood

In vivo PFC5 concentration profiles in blood were evaluated in Balb/c female mice (6 weeks old). 100 μL of PFC-emulsion was intravenously administered via lateral tail veins. The emulsions' PFC5 concentrations ranged from 0.429 to 0.670 vol.%. Blood (44 μL) was collected with a heparinized blood-collecting glass tube, and mixed with 500 μL of heparin solution in a capped sample tube of the (2) gas chromatograph system.

3. Results

3.1. General characteristics of the emulsion-preparation method with a bath-type sonicator

In representative conditions, we successfully obtained PFC5-containing nano-sized emulsions having diameters of ca. 200 nm in considerably high PFC5 yields. Fig. 3(a) and (b) shows diameter distributions measured by means of dynamic light scattering (DLS) for PEG-P(Asp(C7F9)59) (F-59% in Table 1). In these conditions, we dissolved 12.0 mg of polymer in 300 μL water (4.0 wt.% solution), and put this polymer solution in a 1.5 mL glass vial, followed by additions of 6 μL (corresponding to 2.0 vol.% of water) of PFC5 and 6 μL of PFC6. Sonication was performed for 3 min in a bath-type sonicator at 40 °C. In the first three preparations (run 6 in Table 2), the cumulant diameter obtained was 205.5 ± 15.8 nm (the average ± standard deviation; $n = 3$), and Fig. 3(a) shows the weight-weighted diameter distribution of one preparation. Almost uniformly distributed emulsions were obtained, and the diameter of the emulsion droplets had a very small size about 200 nm. In this run 6, PFC5 concentrations were 0.682 ± 0.074 vol.%. These values are considered large enough for ultrasound images (Kawabata et al., 2005, 2010a,b). In another set of three preparations (on another day, run 7 in Table 2), we obtained a very similar average diameter, 173.5 ± 24.5 nm (the average ± standard deviation; $n = 3$) and PFC5 concentrations. The diameter distribution of one preparation of run 7 is shown in Fig. 3(b). These two figures exhibited a major peak at about 200 nm, while a minor peak was seen in a larger diameter side and a smaller diameter side, as shown in Fig. 3(a) and (b), respectively. This difference may result from a slight variation in sonication conditions such as the position of samples and the water level of the sonicator. These emulsions were obtained and measured without any purification process after the sonication, and a large majority of the emulsions in weight were found to have a diameter of about 200 nm. All these results clearly indicate that this sonication method brought about very small nanometer-sized PFC5-containing emulsions with considerably high PFC5 concentrations.

We measured a proportion of polymer incorporated in the PFC-emulsion out of the feed polymer amount. In these preparation conditions (run 7 in Table 2), 75.4 ± 2.6% ($n = 3$) of the feed polymer was found in a supernatant obtained after centrifugation. (All the PFC-emulsions were observed to precipitate in this centrifugation.) When this measurement was carried out for the polymer alone, 93.8 ± 2.0% ($n = 3$) of the feed polymer was found in a supernatant obtained after centrifugation. Therefore, 18.4% (=93.8%–75.4%) of the feed polymer was considered to be incorporated into the PFC-emulsions. Removal of the free polymer chain, that was not incorporated into the PFC-emulsion, was not examined in this study. The removal is difficult because the free polymer existed as a polymeric micelle was close to the PFC-emulsion in size. (If the free polymer existed as a single polymer chain, a difference in size between the free polymer and the PFC-emulsion would be so large to allow separation such as ultrafiltration.)

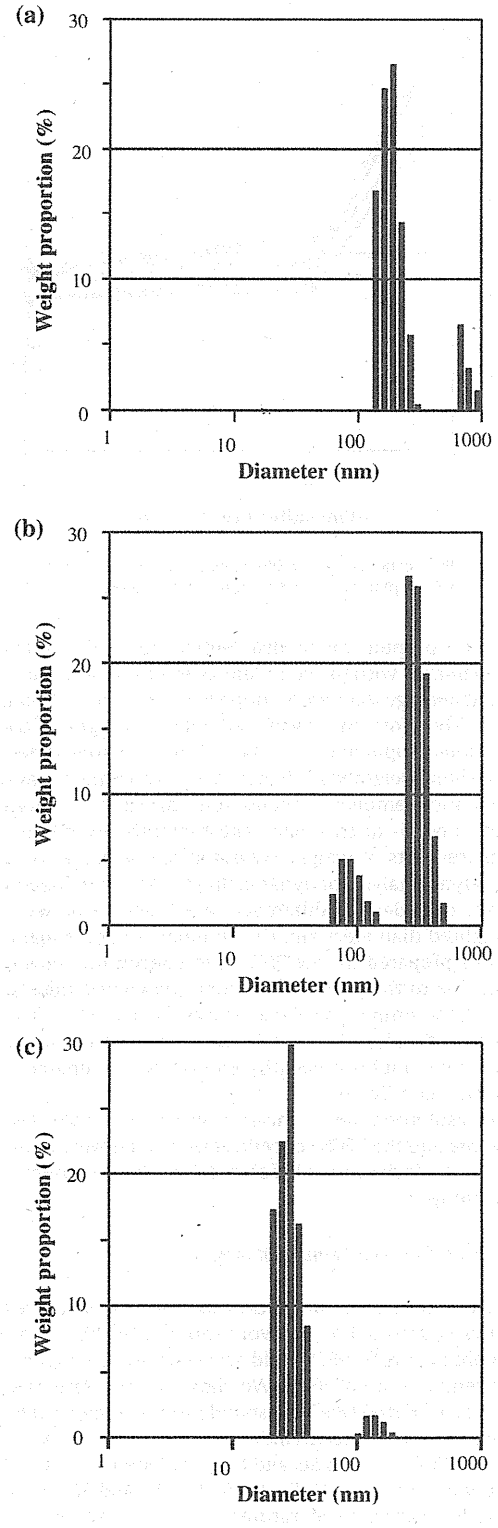

Fig. 3. Diameter distribution of PFC5-containing nano-emulsions (a and b) forming from PEG-P(Asp(C7F9)59) and empty polymeric micelle (c) measured by means of DLS. (a and b) are of different batches but prepared in the same conditions.

Using this polymer amount incorporated into the PFC-emulsions, we calculated the thickness of the polymer shell. We carried out the calculation with the following assumptions.

(1) The PFC-emulsions are made of the two phases; the inner PFC droplet phase and the outer polymer shell phase.
(2) We obtained PFC6 amounts in the emulsions assuming that sensitivity of PFC6 in gas chromatography is the same as that of PFC5. (The same peak area per PFC volume.)
(3) PFC6 and PFC5 are mixed freely without any gain or loss of droplet volume.
(4) Density of polymer is 1.03. (This is a common value of protein, and most synthetic polymers show similar values.)

The obtained value of the polymer shell's thickness was 22 nm, while the radius of the PFC droplet was 65 nm. In the future study, we like to analyse relationships between the shell thickness and physical stability of the emulsions.

3.2. Comparison with other emulsion-preparation methods

We compared the PFC5's concentrations of the PFC5-containing emulsions prepared in the sonication method with the PFC5's concentrations of the emulsions prepared in two common methods; mechanical stirring and high-pressure emulsification (Solans et al., 2005). We also compared the diameters of the emulsions prepared in the sonication method with those prepared in the two common methods. Previously, we reported PFC5-containing emulsions prepared by means of mechanical stirring that featured a magnetic stirrer (Nishihara et al., 2009). In this method, only the F-14% polymer provided a high PFC5 concentration (0.65 vol.%). The other polymers provided low or very low PFC5 concentrations: F-6% had 0.28 vol.%, F-22% had 0.19 vol.%, F-39% had 0.02 vol.%, and F-67% had 0.01 vol.%. In the F-14% case, the cumulant diameter was 694 nm, which was much larger than those obtained in the sonication method as described in the previous section (Section 3.1). Another distinct difference was found in a wide range of polymer compositions for high PFC5 concentrations in the sonication method. As summarized in runs 1–5 of Table 2, we compared the PFC5 concentrations (vol.%) and average diameters of the PFC5-containing emulsions for five polymer compositions. All these five compositions of polymers provided high PFC5 concentrations larger than 0.6 vol.%. Furthermore, all emulsion sizes of these runs (runs 2–5) were revealed to be small, at about 200 nm.

In the next step, we compared the sonication method with the most common method for emulsion preparation:high-pressure emulsification. For this comparison, we used F-15% polymer. We compared PFC5 concentrations and the cumulant average diameters of the emulsions prepared in the sonication method with PFC5 concentrations and the cumulant average diameters of the "high-pressure method" emulsions. We acquired a considerably high PFC5 concentration, 0.58 vol.%, by using a high-pressure emulsifier for the high-pressure emulsification method (its procedure is described in Section 2.3.1). However, the cumulant average diameter of the obtained emulsion was 477 nm. This value was much larger than the sonication-method value (232.4 nm, run 2 of Table 2). Additionally, maintenance of a low temperature at 4 °C for the whole instrument was essential in the high-pressure emulsification method, since possible heat generation due to the high-pressure process may considerably boost evaporation of PFC5 (the boiling temperature of PFC5 is 29 °C). In contrast, in the sonication method, a high PFC5 concentration was obtained at 40 °C, which is above PFC5's boiling temperature. (The temperature issue of the emulsion-preparation process will be more closely examined in the following section (Section 3.4).)

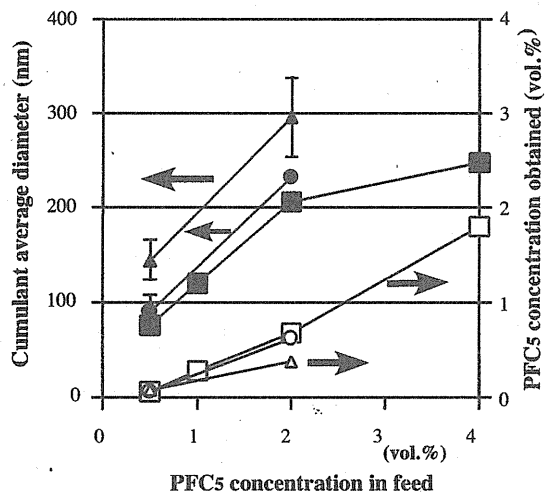

Fig. 4. Effects of polymer and PFC5 concentrations on physical properties of emulsions. PEG-P(Asp(C7F9)59) was used for emulsion preparations. Sample volume was 300 μL in 1.5-mL sample vials. Sonication was performed for 3 min at 40 °C. Filled plots represent cumulant average diameters, and vacant plots represent PFC5 concentrations of emulsions. Polymer concentration: △, ▲: 1.0 vol.%; ○, ●: 2.0 vol.%; □, ■: 4.0 vol.%.

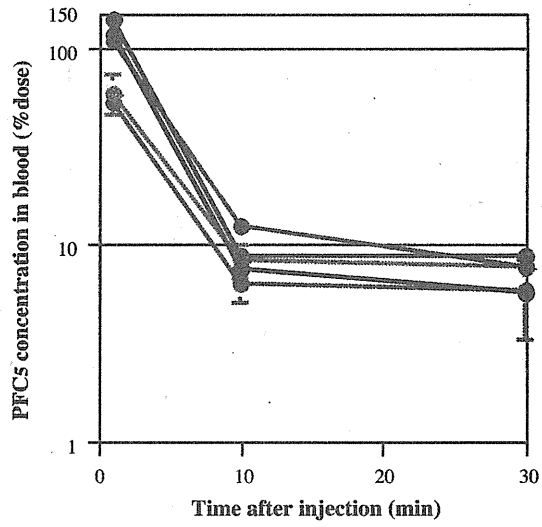

Fig. 5. Profiles of PFC5 concentration in blood. Black plot: run 1; blue plot: run 2; green plot: run 3; yellow plot: run 4; and red plot: run 5 (Table 5).

All these results indicate that the sonication method is a facile method for preparations of PFC5-containg emulsions with very small nano-sizes and high PFC5 concentrations.

3.3. *Effects of sample volume, polymer concentration, and PFC5 concentration on incorporation behaviors*

In the standard conditions, we put 300 μL water in a 1.5-mL of sealed glass tube and added polymer, PFC5, and PFC6. This configuration meant that a considerable amount of PFC5 perhaps would move from the solution into the glass tube's vacant atmospheric space (ca. 1.2 mL). We changed the volume of water while keeping constant the concentrations of polymer, PFC5, and PFC6 in the tube. Table 2 summarizes the results of runs 6–9 of Table 2. A higher PFC5 concentration was obtained in a case involving a larger water volume. (This means that there was a smaller vacant space in a sealed tube.) In accordance with the higher concentration of PFC5, the average diameter of the emulsion was observed to be larger. In run 9, PFC5's yield reached a very high value, approximately 90%. On the other hand, the PFC5's yield decreased to 32–33% when a small sample volume (300 μL) was adopted. These values indicate that the emulsification process can be well controlled through adjustment of sample volume.

Then, we examined effects that both polymer concentrations and PFC5 concentrations in feed had on the two physical values: diameter and PFC5 concentrations of the emulsion. Fig. 4 shows results of these two physical values for F-59% polymer cases. We changed the polymer concentration and the PFC5 concentration in feed in a range of 1.0–4.0 wt.% and of 0.5–4.0 vol.%, respectively. Each empty plot indicates PFC5 concentrations obtained for each polymer concentration, while each filled plot indicates cumulant average diameters for each polymer concentration. The polymer concentration was not found to significantly affect these two physical values. The polymer concentration affected very slightly the PFC5 content because three plot lines almost overlapped. When the polymer concentration was raised, only a small drop in the cumulant average diameter was observed. In contrast, the PFC5 concentration in feed was revealed to greatly affect the two physical values; larger values of PFC5 concentrations and cumulant average diameters were obtained with larger PFC5 concentrations in feed. Diameters of multi-modal distributions like Fig. 3(a) and (b) cannot be evaluated with the cumulant average diameters because the cumulant average diameters suppose the uni-modal diameter distribution. Therefore, we evaluated weight-weighted diameter distributions. Supplementary data, Table A summarizes and compares weight-weighted diameters with the cumulant average diameters. In most emulsion preparations, diameter distributions were found to be bi- or tri-modal, and therefore, exactly quantitative measurements of weight-weighted diameters are difficult in the homodyne analysis of dynamic light scattering done in this study. In fact, considerable differences are observed between the weight-weighted diameters and the cumulant average diameters for emulsions prepared in low PFC5 feed concentrations such as 1%, possibly due to the presence of empty polymeric micelles. (A DLS result of the empty micelle is shown in Fig. 3(c).) Even in this technical difficulty, the correlations obtained in Fig. 4a are not changed when multi-modal distributions are compared in the Supplementary data, Table A.

From the results obtained in this section, it was revealed that the sample volume and the PFC5 concentration in feed were appropriate factors for the facile control of size and the PFC5 content of the nano-sized emulsion.

3.4. *Function of PFC6 in an emulsion preparation*

In the above-described procedures for the emulsion preparation, we always used a 1:1 (vol./vol.) mixture of PFC5 and PFC6 in order to obtain a high PFC5 yield at a temperature higher than the boiling temperature of PFC5. We chose this 1:1 ratio because Kawabata et al. reported that ultrasound intensity required for the phase-transition (vaporization) induction at the 1:1 ratio was similar to that of a PFC5 alone case, and that this intensity was almost constant between ratios of 15:85, 50:50 (=1:1), and 85:15 (Asami et al., 2009). We varied temperatures (15, 25, 40, and 65 °C) of a sonicator's water bath, and performed the emulsion preparation both in the presence and the absence of PFC6 at each temperature. Table 3 summarizes results. In the absence of PFC6, PFC5 concentration was smaller than that of the corresponding PFC6-present case at every temperature. In runs 2 and 4, the obtained emulsions contained a considerable quantity of PFC5 over 0.2 vol.%. These two runs were prepared at lower temperatures than a boiling temperature of PFC5 (29 °C). Only a very small amount of PFC5

Table 3
Effects of temperature and PFC6 addition on PFC5 incorporation behaviors.

Run	Temperature (°C)	PFC6 addition	PFC5 concentration (vol.%)[a]	Cumulant average diameter (nm)[a]
1	15	Yes	0.727 ± 0.191	210.8 ± 17.8
2	15	No	0.419 ± 0.124	82.7 ± 2.6
3	25	Yes	0.566 ± 0.367	177.1 ± 8.9
4	25	No	0.205 ± 0.086	95.7 ± 8.9
5[b]	40	Yes	0.634 ± 0.361	173.5 ± 24.5
6	40	No	0.049 ± 0.059	98.5 ± 5.1
7	65	Yes	0.154 ± 0.051	136.2 ± 16.0
8	65	No	0.096[c]	303.7[c]

[a] Average ± standard deviation ($n = 3$) except run 8.
[b] This run is identical to run 6 of Table 2.
[c] Average of two preparations.

was incorporated in run 6, which was performed at 40 °C, which is above PFC5's boiling temperature. This indicates that most PFC5 evaporated at 40 °C, and that interfacial Laplace pressure did not suppress PFC5's evaporation in the sonication procedure possibly because PFC5 evaporated from macroscopic PFC's droplets (in mm scale) before its incorporation into nano-emulsions where Laplace pressure's effect is great. In contrast, the PFC6-present cases presented similar amounts of PFC5 incorporated at 15, 25, and 40 °C. This means that PFC5's evaporation at 40 °C was efficiently suppressed through the mixing with PFC6. PFC5 and PFC6 not only are miscible but also these two compounds are expected to strongly interact with each other because these are both perfluorocarbons. It is considered that PFC5 evades evaporation through the strong interaction with PFC6 that has a higher boiling temperature than 40 °C. In run 7, performed at 65 °C, a considerable drop in the incorporated PFC5 amount was seen. This sonication temperature (65 °C) is higher than PFC6's boiling temperature (60 °C), and therefore, both PFC5 and PFC6 were evaporated at 65 °C. From these results, we have confirmed the function of the added PFC6 for high PFC5-incorporation amounts at a temperature higher than PFC5's boiling temperature.

3.5. PFC5 concentration profile in blood

We measured PFC concentrations in blood using several PFC5-containing emulsions in order to control their pharmacokinetic behaviors. For a larger amount of emulsion accumulation at tumor tissues, a longer half-life is preferable for a contrast agent. In contrast, a shorter half-life is advantageous for a diagnosis in a short period after injection of a contrast injection, since a low concentration of the contrast agent in blood is a pre-requisite for a high contrast image of the contrast agent's accumulated region. Under this contradictory situation for the optimum half-life, it is very important to obtain technologies to control (prolong and shorten) a half-life of the contrast agent.

We used three different types of polymers including PEG-P(Asp(C7F9)x) block copolymers in order to control half-livers in blood. In Table 4, we describe the compositions of the two copolymers other than PEG-P(Asp(C7F9)x). These two copolymers contain hydrophobic poly(L-lactic acid) chains that are expected to work for incorporation of hydrophobic PFC5 into emulsions. Table 5 summarizes five samples prepared from four polymers. By adjusting the vacant volume of a 1.5-mL glass vial to a small value (ca., 300 μL, meaning 1.2 mL of the sample volume.), we successfully obtained emulsions with higher PFC5 contents than 0.4 vol.% in runs 1–3. In these cases, the sonication was carried out at 15 °C. When emulsions were prepared in the same conditions of run 1 except for a different temperature (at 40 °C) and a different vacant volume (ca. 0 μL), the PFC5 content was considerably lower (0.408 vol.%) than in run 1.

Table 4
Compositions of two poly(L-lactic acid)(PLA)-containing polymers.

Code	Structure	Compositions
Gelatin derivative	Poly(L-lactic acid)-grafted gelatin	M.W. of PLA: 1000 weight ratio PLA/gelatin = 0.17
PEG-PLA	Poly(ethylene glycol)-b-Poly(L-lactic acid) Block copolymer	M.W. of PEG: 2000 M.W. of PLA: 1000

We injected these five samples in a mouse tail vein. As shown in Fig. 5, we observed a distinct difference in PFC5 concentrations at 1 min after the injection between three runs containing PLA (runs 1–3) and the other two runs for PEG-P(Asp(C7F9)x). The former three runs showed almost a 100% dose at 1 min with an assumption that blood volume was 7 vol./wt.% of body weight, while the latter two runs provided considerably smaller values than the 100% dose. In all runs, however, PFC5 concentrations were rapidly lowered at 10 and 30 min after the injection, and no clear difference was observed at these time points among all the runs. Therefore, control of pharmacokinetic behaviors, in particular prolongation of blood half-life from a few minutes, was not successfully achieved in this examination by the use of different polymer structures. For the pharmacokinetic control of the emulsions, an additional functional component may be required. Rapoport et al. (Rapoport et al., 2011) reported a very stable circulation (half-life = 2–4 h) in blood for perfluoro-crown-ether compound containing nano-emulsions.

Table 5
Compositions of PFC-emulsions for in vivo experiments.

Run	Polymer	Polymer concentration in feed (%)[a]	PFC5 concentration in feed (vol.%)	PFC5 concentration obtained in emulsion (vol.%)	Cumulant average diameter (nm)
1	Gelatin derivative[b]	1.0	1.25[d]	0.613	345.9
2	Gelatin derivative[b]	4.0	1.25[d]	0.429	542.6
3	PEG-b-PLA[a]	4.0	1.0[d]	0.491	222.6
4	F-15%[c]	4.0	2.0	0.465	256.3
5	F-59%[c]	4.0	1.0	0.670	225.1

[a] Weight (g)/water volume (mL).
[b] Listed in Table 4.
[c] Listed in Table 1.
[d] Sonication at 15 °C.

According to this report, a perfluoro compound showing stable emulsion formation may be utilized for stable incorporation of another PFC.

4. Discussion

In the examinations of this study, we successfully obtained very small (ca. 200 nm in diameter) PFC5-containing emulsions with high PFC5 contents in a very facile method using a common bath-type sonicator. Actually, the used sonicator was the smallest model with the lowest sonication power (max. Input power: 90 W) in its product line. The other facile aspect of this preparation method is the working temperature. By mixing PFC6 we performed the emulsion preparation at 40 °C, which is above the boiling temperature of PFC5. In a conventional method's use of a high-pressure emulsifier, cooling of the whole system is required for evading a large amount evaporation of PFC5 due to heat generated within a high-pressure emulsifier. In contrast, we did not need cooling samples during the preparation. This facileness is substantially important when we consider a scale-up of the emulsion preparations. In a large-scale production of these emulsions, the heat generated in preparation processes (both in emulsification and sonication) may become large enough to raise a temperature of the solution above the boiling temperature. Therefore, successful preparations at a high temperature means that there is a large margin for large-scale preparation with high PFC5 content as well as easy handling of samples at room temperature throughout the sonication procedure.

We could not substantially change pharmacokinetic behaviors of the PFC5-containing emulsion, even when using different polymers. This is a very different situation from polymeric micelle drug carrier cases where block polymer structure was revealed to be a very influential factor on pharmacokinetic behaviors of the incorporated drug into the polymeric micelles (Yokoyama, 2005, 2007; Watanabe et al., 2006). This difference may result from the liquid state of the emulsion's core, while the solid core is essential for stable drug incorporation in the polymeric micelle systems. An alternative and novel method may be required to obtain stable incorporation of liquid PFC for dramatically changed pharmacokinetics.

5. Conclusion

By using a bath-type sonicator, we successfully obtained PFC5-containing emulsions in a diameter range of 200 nm. These emulsions are very potent for theranostics of solid tumors through ultrasound irradiation. Furthermore, these emulsions were prepared in high PFC5 yields at 40 °C, which is higher than the boiling temperature of PFC5. This very facile preparation method is an important technological key for large-scale production of these medically valuable emulsions.

Acknowledgements

This work was supported by the New Energy and Industrial Technology Development Organization, Japan. M. Yokoyama, K. Shiraishi, and M. Nishihara acknowledge support from the JST CREST program, Grant-in-Aid of the Ministry of Education, Culture, Sports, Science and Technology, Japan, and Kanagawa Academy of Science and Technology. The authors acknowledge Dr. Kenichi Kawabata and Dr. Rei Asami of Central Research Laboratory, Hitachi, Ltd., for their valuable discussion on PFC-containing nanoemulsions.

Appendix A. Supplementary data

Supplementary data associated with this article can be found, in the online version, at doi:10.1016/j.ijpharm.2011.10.006.

References

Ai, H., 2011. Layer-by-layer capsules for magnetic resonance imaging and drug delivery. Adv. Drug Deliv. Rev. 63, 772–788.
Asami, R., Azuma, T., Kawabata, K., 2009. Fluorocarbon droplets as next generation contrast agents—their behavior under 1–3 mhz ultrasound. IEEE Proc. Int. Ultrasonics Symp., 1294–1297.
Asami, R., Ikeda, T., Azuma, T., Kawabata, K., Umemura, S., 2010. Acoustic signal characterization of phase change nanodroplets in tissue-mimicking phantom gels. Jpn. J. Appl. Phys. 49, 07HF16.
Blanco, E., Kessinger, C.W., Sumer, B.D., Gao, J., 2009. Multifunctional micellar nanomedicine for cancer therapy. Exp. Biol. Med. 234, 123–131.
Bryson, J.M., Fichter, K.M., Chu, W.J., Lee, J.H., Li, J., Madsen, L.A., McLendon, P.M., Reineke, T.M., 2009. Polymer beacons for luminescence and magnetic resonance imaging of DNA delivery. Proc. Natl. Acad. Sci. U.S.A. 106, 16913–16918.
Chen, X.S., 2011. Introducing theranostics journal—from the editor-in-chief. Theranostics 1, 1–2.
Gianella, A., Jarzyna, P.A., Mani, V., Ramachandran, S., Calcagno, C., Tang, J., Kann, B., Dijk, W.J., Thijssen, V.L., Griffioen, A.W., Storm, G., Fayad, Z.A., Mulder, W.J., 2011. A multifunctional nanoemulsion platform for imaging guided therapy evaluated in experimental cancer. ACS Nano 5, 4422–4433.
Grishenkov, D., Pecorari, C., Brismar, T.B., Paradossi, G., 2009. Characterization of acoustic properties of PVA-shelled ultrasound contrast agents: ultrasound-induced fracture (part II). Ultrasound Med. Biol. 35, 1139–1147.
Hernot, S., Klibanov, A.L., 2008. Microbubbles in ultrasound-triggered drug and gene delivery. Adv. Drug Deliv. Rev. 60, 1153–1166.
Ishida, O., Maruyama, K., Sasaki, K., Iwatsuru, M., 1999. Size-dependent extravasation and interstitial localization of polyethyleneglycol liposomes in solid tumor-bearing mice. Int. J. Pharm. 190, 49–56.
Jeong, H., Huh, M., Lee, S.J., Koo, H., Kwon, I.C., Jeong, S.Y., Kim, K., 2011. Photosensitizer-conjugated human serum albumin nanoparticles for effective photodynamic therapy. Theranostics 1, 230–239.
Kaida, S., Cabral, H., Kumagai, M., Kishimura, A., Terada, Y., Sekino, M., Aoki, I., Nishiyama, N., Tani, T., Kataoka, K., 2010. Visible drug delivery by supramolecular nanocarriers directing to single-platformed diagnosis and therapy of pancreatic tumor model. Cancer Res. 70, 7031–7041.
Kalber, T.L., Kamaly, N., Higham, S.A., Pugh, J.A., Bunch, J., McLeod, C.W., Miller, A.D., Bell, J.D., 2011. Synthesis and characterization of a theranostic vascular disrupting agent for in vivo MR imaging. Bioconjug. Chem. 22, 879–886.
Kamaly, N., Miller, A.D., 2010. Paramagnetic liposome nanoparticles for cellular and tumour imaging. Int. J. Mol. Sci. 11, 1759–1776.
Kawabata, K., Sugita, N., Yoshikawa, H., Azuma, T., Umemura, S., 2005. Nanoparticles with multiple perfluorocarbons for controllable ultrasonically induced phase shifting. Jpn. J. Appl. Phys. 44, 4548–4552.
Kawabata, K., Asami, R., Yoshikawa, H., Azuma, T., Umemura, S., 2010a. Acoustic response of microbubbles derived from phase-change nanodroplet. Jpn. J. Appl. Phys. 49, 07HF18.
Kawabata, K., Asami, R., Yoshikawa, H., Azuma, T., Umemura, S., 2010b. Sustaining microbubbles derived from phase change nanodroplet by low-amplitude ultrasound exposure. Jpn. J. Appl. Phys. 49, 07HF20.
Kim, K., Kim, J.H., Park, H., Kim, Y.S., Park, K., Nam, H., Lee, S., Park, J.H., Park, R.W., Kim, I.S., Choi, K., Kim, S.Y., Park, K., Kwon, I.C., 2010. Tumor-homing multifunctional nanoparticles for cancer theragnosis: simultaneous diagnosis, drug delivery, and therapeutic monitoring. J. Contr. Rel. 146, 219–227.
Lammers, T., Kiessling, F., Hennink, W.E., Storm, G., 2010. Nanotheranostics and image-guided drug delivery: current concepts and future directions. Mol. Pharm. 7, 1899–1912.
Lammers, T., Aime, S., Hennink, W.E., Storm, G., Kiessling, F., 2011. Theranostic Nanomedicines. Acc. Chem. Res. 44, 1029–1038.
Litzinger, D.C., Buiting, A.M.J., van Rooijen, N., Huang, L., 1994. Effect of liposome size on the circulation time and intraorgan distribution of amphipathic poly(ethylene glycol)-containing liposomes. Biochim. Biophys. Acta 1190, 99–107.
MacKay, J.A., Li, Z., 2010. Theranostic agents that co-deliver therapeutic and imaging agents? Adv. Drug Deliv. Rev. 62, 1003–1004.
Min, K.H., Kim, J.H., Bae, S.M., Shin, H., Kim, M.S., Park, S., Lee, H., Park, R.W., Kim, I.S., Kim, K., Kwon, I.C., Jeong, S.Y., Lee, D.S., 2010. Tumoral acidic pH-responsive MPEG-poly(beta-amino ester) polymeric micelles for cancer targeting therapy. J. Contr. Rel. 144, 259–266.
Mohan, P., Rapoport, N., 2010. Doxorubicin as a molecular nanotheranostic agent: effect of doxorubicin encapsulation in micelles or nanoemulsions on the ultrasound-mediated intracellular delivery and nuclear trafficking. Mol. Pharm. 6, 1959–1973.
Moon, G.D., Choi, S.W., Cai, X., Li, W., Cho, E.C., Jeong, U., Wang, L.V., Xia, Y., 2011. A new theranostic system based on gold nanocages and phase-change materials with unique features for photoacoustic imaging and controlled release. J. Am. Chem. Soc. 133, 4762–4765.
Nagayasu, A., Uchiyama, K., Nishida, T., Yamagiwa, Y., Kawai, Y., Kiwada, H., 1996. Is control of distribution of liposomes between tumors and bone marrow possible? Biochim. Biophys. Acta 1278, 29–34.
Nakamura, E., Makino, K., Okano, T., Yamamoto, T., Yokoyama, M., 2006. A polymeric micelle MRI contrast agent with changeable relaxivity. J. Contr. Rel. 114, 325–333.
Nishihara, M., Imai, K., Yokoyama, M., 2009. Preparation of perfluorocarbon/fluoroalkyl polymer nanodroplets for cancer-targeted ultrasound contrast agents. Chem. Lett. 38, 556–557.

Opanasopit, P., Yokoyama, M., Watanabe, M., Kawano, K., Maitani, Y., Okano, T., 2004. Block copolymer design for camptothecin incorporation into polymeric micelles for passive tumor targeting. Pharm. Res. 21, 2003–2010.
Pan, D., Caruthers, S.D., Hu, G., Senpan, A., Scott, M.J., Gaffney, P.J., Wickline, S.A., Lanza, G.M., 2008. Ligand-directed nanobialys as theranostic agent for drug delivery and manganese-based magnetic resonance imaging of vascular targets. J. Am. Chem. Soc. 130, 9186–9187.
Rapoport, N., Gao, Z., Kennedy, A., 2007. Multifunctional nanoparticles for combining ultrasonic tumor imaging and targeted chemotherapy. J. Natl. Cancer Inst. 99, 1095–1106.
Rapoport, N.Y., Kennedy, A.M., Shea, J.E., Scaife, C.L., Nam, K.H., 2009a. Controlled and targeted tumor chemotherapy by ultrasound-activated nanoemulsions/microbubbles. J. Contr. Rel. 138, 268–276.
Rapoport, N.Y., Nam, K.H., Gao, Z., Kennedy, A., 2009b. Application of ultrasound for targeted nanotherapy of malignant tumors. Acoust. Phys. 55, 594–601.
Rapoport, N., Christensen, D.A., Kennedy, A.M., Nam, K.H., 2010a. Cavitation properties of block copolymer stabilized phase-shift nanoemulsions used as drug carriers. Ultrasound Med. Biol. 36, 419–429.
Rapoport, N., Kennedy, A.M., Shea, J.E., Scaife, C.L., Nam, K.H., 2010b. Ultrasonic nanotherapy of pancreatic cancer: lessons from ultrasound imaging. Mol. Pharm. 7, 22–31.
Rapoport, N., Nam, K.H., Gupta, R., Gao, Z., Mohan, P., Payne, A., Todd, N., Liu, X., Kim, T., Shea, J., Scaife, C., Parker, D.L., Jeong, E.K., Kennedy, A.M., 2011. Ultrasound-mediated tumor imaging and nanotherapy using drug loaded, block copolymer stabilized perfluorocarbon nanoemulsions. J. Contr. Rel. 153, 4–15.
Sanson, C., Diou, O., Thévenot, J., Ibarboure, E., Soum, A., Brûlet, A., Miraux, S., Thiaudière, E., Tan, S., Brisson, A., Dupuis, V., Sandre, O., Lecommandoux, S., 2011. Doxorubicin loaded magnetic polymersomes: theranostic nanocarriers for MR imaging and magneto-chemotherapy. ACS Nano 5, 1122–1140.
Schutt, E.G., Klein, D.H., Mattrey, R.M., Riess, J.G., 2003. Injectable microbubbles as contrast agents for diagnostic ultrasound imaging: the key role of perfluorochemicals. Angew. Chem. Int. Ed. Engl. 42, 3218–3235.
Shiraishi, K., Kawano, K., Minowa, T., Maitani, Y., Yokoyama, M., 2009. Preparation and in vivo imaging of PEG-poly(L-lysine)-based polymeric micelle MRI contrast agents. J. Contr. Rel. 136, 14–20.
Shiraishi, K., Kawano, K., Maitani, Y., Yokoyama, M., 2010. Synthesis of Poly(ethylene glycol)-b-poly(L-lysine) block copolymers having Gd-DOTA as MRI contrast agent and their polymeric micelle formation by polyion complexation. J. Contr. Rel. 148, 160–167.
Solans, C., Izquierdo, P., Nolla, J., Azemar, N., Garcia-Celma, M.J., 2005. Nano-emulsions. Curr. Opin. Colloid Interface Sci. 10, 102–110.
Tadros, T., Izuquierdo, P., Esquena, J., Solans, C., 2004. Formation and stability of nano-emulsions. Adv. Colloid Interface. Sci. 108–109, 303–318.
Tanigo, T., Takaoka, R., Tabata, Y., 2010. Sustained release of water-insoluble simvastatin from biodegradable hydrogel augments bone regeneration. J. Contr. Rel. 143, 201–206.
Unger, E.C., Porter, T., Culp, W., Labell, R., Matsunaga, T., Zutshi, R., 2004. Therapeutic applications of lipid-coated microbubbles. Adv. Drug Deliv. Rev. 56, 1291–1314.
Yamamoto, T., Yokoyama, M., Opanasopit, P., Hayama, A., Kawano, K., Maitani, Y., 2007. What are determining factors for stable drug incorporation into polymeric micelle carriers? Consideration on physical and chemical characters of the micelle inner core. J. Contr. Rel. 123, 11–18.
Yokoyama, M., 2005. Polymeric micelles for the targeting of hydrophobic drugs, In: Kwon, G.S. (Ed.), Drug and Pharmaceutical Sciences, Polymeric Drug Delivery Systems, 148. Taylor & Francis, Boca Raton, pp. 533–575.
Yokoyama, M., 2007. Polymeric micelles as nano-sized drug carrier systems. In: Domb, A.J., Tabata, Y., Kumar, M.N.V.R., Farber, S. (Eds.), Nanoparticles for Pharmaceutical Applications. American Scientific Publishers, Stevenson Ranch, pp. 63–72.
Yokoyama, M., Opanasopit, P., Maitani, Y., Kawano, K., Okano, T., 2004. Polymer design and incorporation method for polymeric micelle carrier system containing water-insoluble anti-cancer agent camptothecin. J. Drug Target. 12, 373–384.
Yuan, F., Dellian, M., Fukumura, D., Leunig, M., Berk, D.A., Torchilin, V.P., Jain, R.K., 1995. Vascular permeability in a human tumor xenograft: molecular size dependence and cutoff size. Cancer Res. 55, 3752–3756.
Watanabe, M., Kawano, K., Yokoyama, M., Opanasopit, P., Okano, T., Maitani, Y., 2006. Preparation of camptothecin-loaded polymeric micelles and evaluation of their incorporation and circulation stability. Int. J. Pharm. 308, 183–189.

International Journal of Cardiology 152 (2011) 202–206

Contents lists available at ScienceDirect

International Journal of Cardiology

journal homepage: www.elsevier.com/locate/ijcard

Enhancement of ultrasonic thrombus imaging using novel liposomal bubbles targeting activated platelet glycoprotein IIb/IIIa complex—*in vitro* and *in vivo* study

Kohsuke Hagisawa [a], Toshihiko Nishioka [b,*], Ryo Suzuki [c], Tomoko Takizawa [c], Kazuo Maruyama [c], Bonpei Takase [d], Masayuki Ishihara [d], Akira Kurita [d], Nobuo Yoshimoto [b], Fumitaka Ohsuzu [e], Makoto Kikuchi [a]

[a] Department of Medical Engineering, National Defense Medical College, 3-2 Namiki, Tokorozawa, Saitama 359-8513, Japan
[b] Division of Cardiology, Saitama Medical Center, Saitama Medical University, 1981 Kamoda, Kawagoe, Saitama 350-8550, Japan
[c] Department of Biopharmaceutics, School of Pharmaceutical Science, Teikyo University, 1091-1 Suwarashi, Sagamiko, Sagamihara, Kanagawa 229-0195, Japan
[d] Division of Biomedical Engineering, National Defense Medical College, 3-2 Namiki, Tokorozawa, Saitama 359-8513, Japan
[e] First Department of Internal Medicine, National Defense Medical College, 3-2 Namiki, Tokorozawa, Saitama 359-8513, Japan

ARTICLE INFO

Article history:
Received 12 February 2010
Received in revised form 19 June 2010
Accepted 4 July 2010
Available online 1 August 2010

Keywords:
Echocardiography
Thrombus
Imaging
Ultrasound
Liposome

ABSTRACT

Background: We developed perfluorocarbon gas-containing bubble liposomes (BL) with Arg-Gly-Asp (RGD) sequence-containing peptides, which bind to activated platelet glycoprotein IIb/IIIa complexes. The aim of this study was to examine the enhancing effects in ultrasonic thrombus imaging using these targeted BL *in vitro* and *in vivo*.

Methods: Liposomes composed of phosphatidylcholine and cholesterol were manufactured, and RGD peptide was attached by a covalent coupling reaction. Sonication was used to conjugate liposomes and perfluorocarbon gas, which formed targeted BL. *In vitro*, targeted BL were mixed with whole blood, which was allowed to coagulate while being shaken and rotated. *In vivo*, we administered targeted BL to 10 rabbits with acute thrombotic occlusions in the ilio-femoral artery. Thrombi were imaged using a 7.5–9 MHz linear transducer and a conventional ultrasound machine, and by scanning electron microscopy. Ultrasound images were digitized, and mean pixel gray-scale level (black = 0, white = 255) was measured.

Results: In vitro, mean pixel gray-scale level of the thrombi in targeted BL group was significantly higher than in control and non-targeted BL groups (93 ± 26 vs. 58 ± 16, 48 ± 9, $p = 0.002$, $n = 10$). Scanning electron microscopy revealed large amounts of targeted BL attached to the thrombi. *In vivo*, mean pixel gray-scale level of the thrombi with targeted BL was significantly higher (33.2 ± 6.4 vs. 24.8 ± 8.5, $p = 0.0051$, $n = 10$) than that before targeted BL administration.

Conclusions: Perfluorocarbon gas-containing BL with RGD peptide represent a novel echo contrast agent, which can markedly enhance ultrasonic thrombus imaging *in vitro* and *in vivo*, and may be useful for noninvasively diagnosing acute thrombotic vessel occlusion.

© 2010 Elsevier Ireland Ltd. All rights reserved.

1. Introduction

Echocardiographic diagnosis of vascular or intracardiac thrombi is sometimes challenging, even using state-of-the-art ultrasound systems and comercially available ultrasound contrast agents [1,2]. Intravascular ultrasound imaging provides more detailed pictures of thrombi due to its higher frequency; however, thrombi within the vessel lumen can often be mistaken for soft plaques, unless they are distinguished from soft plaques by mobility, lobular edges and movement away from the vessel wall during the cardiac cycle [3]. Therefore, it is essential to improve the diagnostic accuracy of echocardiography for detecting thrombi *in vivo*.

Recently, using emerging molecular imaging techniques, several types of novel thrombus-targeting ultrasound contrast agents have been developed and examined for use in the diagnosis of thrombi *in vitro* and in animal models [4–10]. These ultrasound contrast agents are lipid-encapsulated perfluorocarbon gas or nongaseous liposomes, and antibodies or peptides are used as specific ligands to fibrin or platelets. However, these agents are not commercially available.

We have developed novel polyethylene glycol-modified liposomal bubbles (bubble liposomes, BL) containing perfluoropropane gas, which can be used as an ultrasound contrast agent [11–13]. We attached targeted ligands for activated platelets to these BL. We used Arg-Gly-Asp (RGD) sequence-containing peptides, which bind to the

* Corresponding author. Tel.: +81 49 228 3587; fax: +81 49 226 5274.
E-mail address: nishioka@saitama-med.ac.jp (T. Nishioka).

0167-5273/$ – see front matter © 2010 Elsevier Ireland Ltd. All rights reserved.
doi:10.1016/j.ijcard.2010.07.016

fibrinogen receptor on the activated platelet membrane glycoprotein IIb/IIIa complex [14–17]. We hypothesized that the activated thrombus-targeting BL would enhance fresh thrombus visualization by conventional transcutaneous ultrasound and may enable diagnosis of acute thrombotic vessel occlusion. The aim of this study was to examine the enhancing effects on ultrasonic imaging of fresh thrombi using these BL *in vitro* and *in vivo*.

2. Materials and methods

2.1. Preparation of thrombus-targeting BL

The lipid-based shell of the perfluorocarbon gas-containing BL was composed of 12.6 mg of 1,2-distearoyl-sn-glycero-phosphatidylcholine (DSPC) (NOF Corp., Tokyo, Japan), 5.1 mg of 1,2-distearoyl-sn-glycero-3-phosphatidyl-ethanolamine-m-poly-ethyleneglycol 2000 maleimide (DSPE-PEG-Mal-2000; Avanti, Alabaster, AL) and 3.0 mg of cholesterol (Sigma-Aldrich Japan, Tokyo, Japan). Liposomes were prepared by reverse phase evaporation [16]. Briefly, a mixture of all reagents was dissolved in 2.0 ml of chloroform and mixed with the same amount of di-isopropyl ether and normal saline. The mixture was sonicated using a probe-type 19.5-kHz ultrasound at 550 W (XL-2020 Sonicator, Misonix, Inc., Farmingdale, NY) and then evaporated at 65 °C using a rotary evaporating system (Tokyo Rika, Tokyo, Japan). After the chemical solvent was completely removed, the size of liposomes was adjusted to be less than 0.2 μm using extruding equipment and a membrane filter (Northern Lipids, Inc., Vancouver, Canada) with sizing filters. To the liposome liquid, 1 mg of linear octapeptide with an amino acid sequence of cysteine–glycine–glycine–glycine–arginine–glycine–aspartic acid–phenyl-alanine (CGGGRGDF) (Operon Biotechnologies, Tokyo, Japan) was added [14,17] and allowed to conjugate to the maleimide on the liposomal surface via thio-ether covalent coupling at room temperature for 2 h. Gel filtration was then used to remove unreacted peptide fragments. Lipid concentration was measured with the Wako Phospholipid C test (Wako Pure Chemical Industries, Osaka, Japan) and the RGD-liposomes were diluted to a final concentration of 20 mg/ml. The RGD-liposomes were sealed in a 5-ml vial and air was exchanged with perfluoropropane gas (Takachiho Chemical Ind. Co., Ltd., Tokyo, Japan), followed by 20-kHz ultrasound treatment using a bath-type sonicating system (Branson model 3510, Emerson, CT) for 5 min to generate RGD-BL [11,12]. Sterilized filtration (0.45 μm) was then performed to remove expanded and oversized BL. Non-targeted BL were also prepared in the same manner, except without the addition of RGD peptides. The diameter of each BL was determined by dynamic laser light-scattering measurements using the ELS-800 particle analyzer (Otsuka Electronics, Osaka, Japan).

2.2. In vitro thrombus imaging

In total, 30 thrombi were used in this *in vitro* study. For preparation of each thrombus, 9 ml of whole blood was collected in a test tube from a healthy volunteer, placed on a seesaw-type shaker and allowed to coagulate at room temperature while being shaken and rotated at a speed of 60 rpm for 1 h. Ten thrombi served as controls, non-targeted BL were added to 10 thrombi and targeted BL were added to the remaining 10 thrombi. Targeted BL or non-targeted BL (100 μl, 20 mg/ml lipid concentration) were added to the test tube after 10 min. The formed thrombi were washed with normal saline, cut into small pieces and placed in a latex tube filled with degassed water. Thrombi were imaged using a 7.5-MHz linear transducer with a conventional ultrasound machine (SONOS2000, Philips Medical Systems, Potomac, MD) (frame rate, 40–50/s; mechanical index, 0.4) in a bath filled with degassed water. As a control, 10 thrombi prepared without BL were also imaged at the same gain setting and ultrasound intensity. For quantitative analysis, the mean video intensity level of whole thrombi was measured on a 256 gray-scale level (black = 0, white = 255) using NIH image software [18].

2.3. Scanning electron microscopic observation of thrombi

Thrombi were prepared as described for the *in vitro* thrombus imaging study. Thrombi with targeted BL, non-targeted BL or saline were fixed in 2% glutaraldehyde in normal saline and dehydrated in a graded ethanol series. Thrombi were further cut and divided into smaller pieces in order to observe the inside as well as the surface. This was followed by critical-point drying and gold sputtering (JEOL JFC-1100, Nippon Denshi, Tokyo, Japan). Specimens were then examined with a conventional scanning electron microscope (JOEL Carry Scope, Nippon Denshi, Tokyo, Japan) at an acceleration voltage of 5 to 15 kV [19].

2.4. Acute thrombotic occlusion model of rabbit ilio-femoral artery

This study followed the American Physiological Society Guidelines for Animal Research, which conform to the "Position of the American Heart Association on Research Animal Use" adopted by the AHA in November 1984. A total of 20 New Zealand white rabbits were used; 10 each for the targeted BL study and the non-targeted BL study. Each rabbit was anesthetized using 50 mg of ketamine and 20 mg of xylazine. Anesthesia was maintained with pentbarbitrate (15 mg/kg). A 5-Fr sheath was inserted into the right carotid artery, a balloon catheter was advanced to the ilio-femoral artery, and the intima was injured by balloon inflation. Afterwards, the balloon catheter was pulled back, a 0.014-inch guide wire was positioned at the injury site, and electrical stimulation (from a 3-V battery) was applied between the guide wire and skin electrode [20,21]. After 30 min, the artery was thrombotically occluded and arterial occlusion was confirmed by angiography.

2.5. In vivo thrombus imaging

The thrombus was imaged in a longitudinal axis view using a 9-MHz linear transducer and a conventional ultrasound machine (UF-750XT, Fukuda Denshi, Ltd., Tokyo, Japan) (frame rate, 24–30/s; mechanical index, 0.3). Manipulating the transducer just above the angiographic vessel occlusion site, the ultrasonic occlusion site was identified as an abrupt interruption of echo-Doppler signal within the vessel. The region of interest was then defined as the area between the near and far vessel walls without a Doppler signal, according to the consensus of two cardiologists (K.H. and T.N.). To maintain the same view, the ultrasound transducer was fixed with a hand-free stabilizer. The ultrasound thrombus images were continuously recorded from just before to 10 min after the bolus injection of targeted BL (1 ml, 20 mg/ml lipid concentration) through the ear vein in 10 rabbits. After the experiment, the video intensity of the thrombus was measured using NIH image, as described for the *in vitro* study. As controls, the video intensity of the thrombi was measured before and after injection of 1 ml (20 mg/ml lipid concentration) of non-targeted (without RGD peptide) BL in another 10 rabbits.

2.6. Statistical analyses

Results are given as means ± 1 standard deviation. As video intensity levels of the thrombi were not considered to be normally distributed, non-parametric tests were used to compare data. For the *in vitro* study, thrombus echo intensity was compared and analyzed using the Kruskal–Wallis test followed by a post-hoc Bonferroni test. For the *in vivo* study, thrombus echo intensity before and after BL administration was compared by the Wilcoxon-signed rank sum test. A p value <0.05 was considered statistically significant.

3. Results

3.1. In vitro thrombus imaging

Ultrasonic images of thrombi were apparently enhanced when compared to the control and non-targeted BL groups (Fig. 1A). The mean pixel gray-scale levels of the control and non-targeted BL thrombi were not significantly different. However, the mean pixel gray-scale level of the thrombi in the targeted BL group was significantly higher than those in the control and non-targeted BL thrombus groups (93 ± 26 vs. 58 ± 16, 48 ± 9, $p = 0.0001$, $n = 10$) (Fig. 1B). Enhancement of ultrasonic thrombus imaging in the targeted BL group lasted at least 15 min, at which point observation was discontinued. BL diameter was 0.185 ± 0.044 μm.

3.2. Scanning electron microscopic observation of thrombi

Large amounts of targeted BL were attached to the fibrin nets and platelets on the surface of thrombi, as well as in the deep inner portions of thrombi (Fig. 2C). In contrast, no BL were attached to the thrombi in the non-targeted BL and control groups (Fig. 2A and B). Targeted BL were smaller than the fibrin mesh (<0.2 μm) in all observed fields.

3.3. In vivo thrombus imaging

The rabbit ilio-femoral arterial thrombus was clearly visualized using a conventional ultrasound system with the targeted BL (Fig. 3A). After targeted BL injection, the mean pixel gray-scale level of the thrombus rapidly peaked (within 1 min) and then gradually decreased; however, it did not return to baseline levels, even after 10 min (Fig. 4). Targeted BL significantly increased the mean pixel gray-scale level of the thrombus at 1 min when compared to that before targeted BL administration (33.2 ± 6.4 vs. 24.8 ± 8.5, $p = 0.0051$, $n = 10$). After non-targeted BL injection, blood echo intensity around the thrombus was increased; however, no significant increases were observed in the

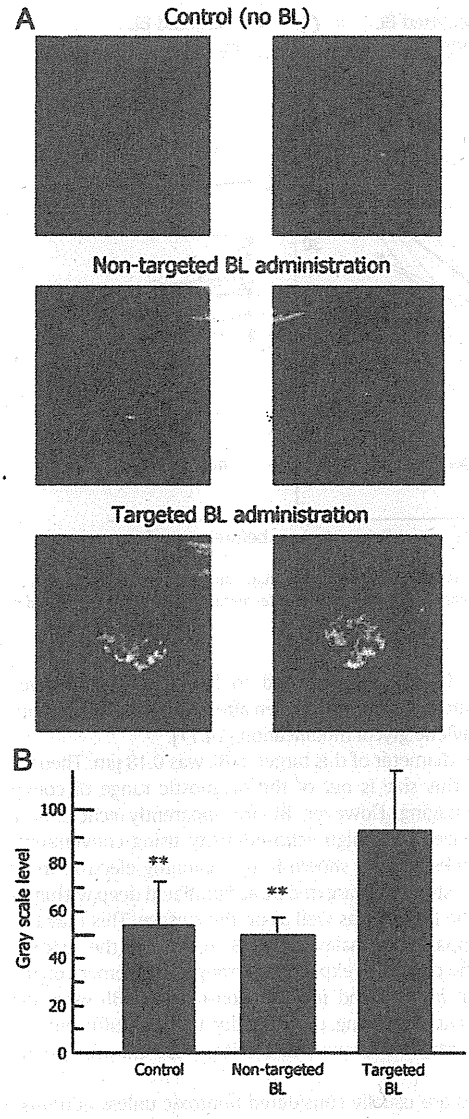

Fig. 1. Ultrasonic thrombus imaging is apparently enhanced by targeted BL *in vitro* when compared to control and non-targeted BL (A). Video intensity levels of the thrombi in the targeted BL group were significantly higher than in the control and non-targeted BL groups (B). BL: bubble liposomes.

mean pixel gray-scale level of the thrombus at 1 min (25.5 ± 4.8 vs. 26.4 ± 5.3, $p = 0.3329$, $n = 10$) (Fig. 3B and C).

4. Discussion

In our *in vitro* and *in vivo* studies, we confirmed that ultrasound imaging of thrombi is markedly enhanced by targeted BL, even via intravenous administration using a conventional diagnostic ultrasound machine. This is also the first study to show the feasibility of perfluorocarbon gas-containing liposomes, rather than a phospholipid mono-layer, as a targeted ultrasound contrast agent, in addition to a carrier for gene delivery [11–13].

In clinical settings, various ultrasound contrast agents with lipid-based or non-lipid-based shells are commercially available for diagnostic use. These agents are prepared to enhance blood flow or tissue perfusion. Some of these agents are capable of passively imaging inflammation using the inherent chemical properties of the shell components [22]. However, they have no specific ligands on their surface for actively targeting pathophysiological molecules.

Lanza et al. first reported a fibrin-targeting ultrasonic contrast agent. They used lipid-encapsulated, nongaseous perfluorocarbon emulsion and an antifibrin monoclonal antibody as a targeting ligand, incorporating avidin-biotin triphasic interaction steps to demonstrate excellent thrombus enhancement [4]. However, this technique has limited applications in humans due to the complexity of targeting interactions and immunogenicity of avidin [23]. Unger et al. developed thrombus-targeting perfluorocarbon gas-containing microbubbles with lipid mono-layer shells incorporating small peptides as ligands for activated platelets [5–7]. This agent was able to enhance ultrasonic thrombus imaging both *in vitro* and *in vivo* during continuous intravenous infusion. Demos and Hamilton reported thrombus-targeting nongaseous echogenic immuno-liposomes, which enhanced ultrasonic imaging of both intravascular and intracardiac thrombi [8,9]. In this study, anti-fibrinogen antibody was used as the targeting ligand, which may cause systemic adverse effects due to secondary immunoreactions. Alonso et al. developed abciximab, an antibody fragment specific for the glycoprotein IIb/IIIa receptor, bearing immunobubbles with phospholipid mono-layer shells. These immunobubbles improved visualization of human clots both *in vitro* and in an *in vivo* model of acute arterial thrombotic occlusion [10].

Targeted BL shows some advantages over these previously reported thrombus-targeting ultrasound contrast agents [4–10]. We used liposomes as a basic structure, as a lipid bi-layer shell increases the stability of BL and works as a barrier against gas diffusion [12], and the liposomal surface can be modified for the conjugation of various targeted ligands, as well as for achieving longer circulation times. Polyethylene glycol was attached to the surface lipid layer in order to

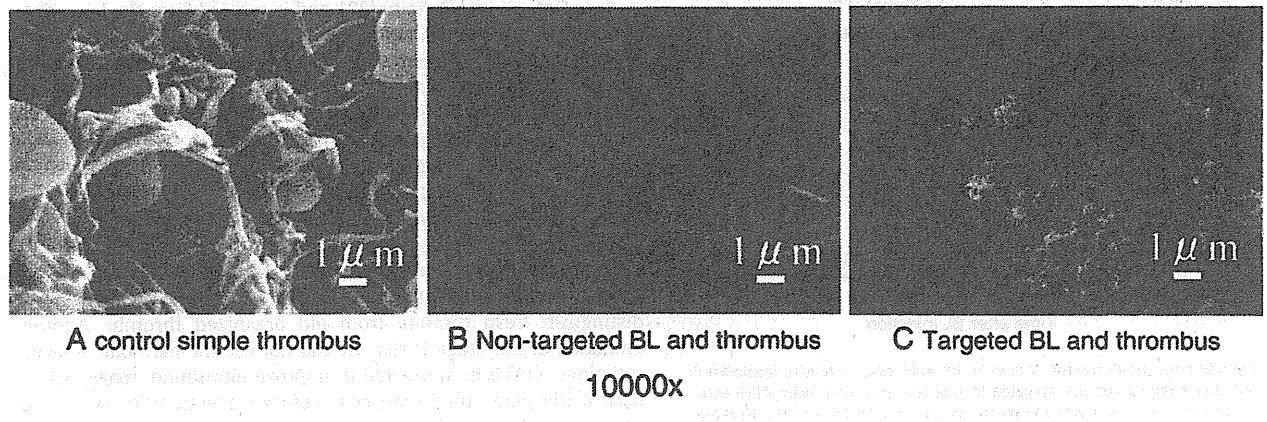

Fig. 2. Scanning electron microscopy revealed large amounts of BL attached to the thrombi in the targeted BL group (C), which were not observed in the non-targeted BL (B) and control groups (A). BL: bubble liposomes.

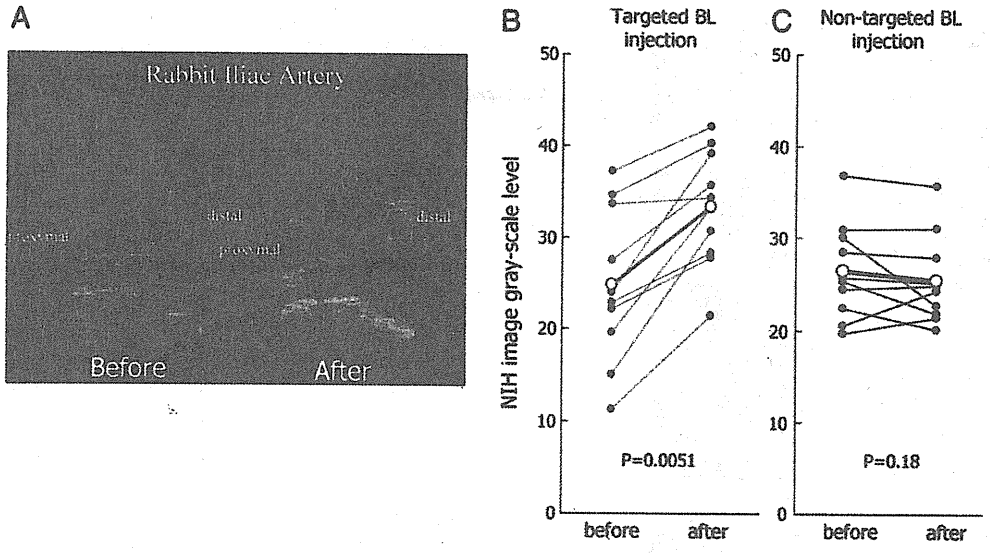

Fig. 3. Ultrasound image of *in vivo* thrombi is significantly enhanced after administration of targeted BL via an ear vein. (A) NIH image quantitative analysis shows significant increases on *in vivo* thrombus echo intensity by intravenous administration of targeted BL; (B) however, similar changes are not seen after administration of non-targeted BL (C). BL: bubble liposomes.

increase hydrophilicity, thereby offering a stealth effect with respect to reticulo-endothelial capture and allowing longer circulation times [24,25]. Moreover, a BL size of less than a micron (nano-size) permits deeper penetration into thrombi.

The targets of ultrasonic thrombus imaging have been fibrin [4,8,9] or activated platelets [5–7,10]. Fibrin is typically present in all types of thrombi (arterial and venous, acute and chronic). In contrast, activated platelets are found in fresh thrombi in cases of acute coronary syndrome and stroke. The RGD sequence-containing peptide is a ligand for the activated platelet membrane glycoprotein IIb/IIIa complex. The RGD peptide is chemically stable and easily conjugated to the lipid surface layer, as it is composed of a small number of amino acids and binds strongly to phospholipids via a thio-ether bond without the need for complex chemical synthesis [14,15]. In contrast to antibodies, peptides are generally smaller in size and simpler in structure, resulting in less immunoreactivity [26,27]. Among the various types of RGD peptides, we used an octapeptide (CGGGRGDF) in this study. The initial C of this peptide was used for coupling and GGG served as an "arm" to distance the active RGD binding site from thiol-coupling to maleimide on the liposomal surface [17]. Moreover, this peptide has been reported to be a potent inhibitor of platelet agglutination through the glycoprotein IIb/IIIa receptor, and to be uniquely sensitive to the activation state of this receptor, even after incorporation into liposomes with polyethylene glycol modification [14,17].

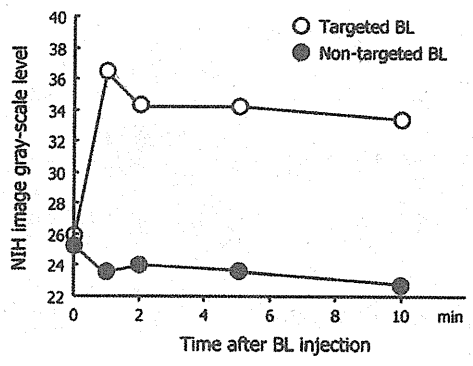

Fig. 4. Representative time-intensity curves of thrombi video intensity immediately before and after targeted and non-targeted BL injection measured using NIH·image. Targeted BL significantly increased the mean pixel gray-scale level of the thrombus from 1 to 10 min after injection; however, no significant increases were observed after non-targeted BL injection. BL: bubble liposomes.

The mean diameter of this targeted BL was 0.18 μm. Theoretically, a single BL of this size is out of the diagnostic range of conventional ultrasound imaging. However, BL are apparently echogenic and are clearly visualized with high echo-intensity using conventional ultrasound machines [11]. As shown in the scanning electron microscopic section of this study, the targeted BL accumulated deep within the inner portions of the thrombi, as well as on the surface. This may have been due to the apparently smaller size of BL relative to the space between fibrin nets, and could also explain the strong enhancement on ultrasonic imaging both *in vitro* and *in vivo*. Non-targeted BL were unable to enhance thrombus imaging, probably due to the insufficient amount of BL passively retained around and within the thrombi required for echogenicity.

Liposomes are usually considered nontoxic unless administered at very high doses [28]. Liposomal drugs are already commercially available and are safely used in humans [29–31]. Polyethylene glycol is also considered nontoxic and is excreted unmetabolized in the urine [32]. The RGD peptide is an octapeptide and is considered to be non-toxic and non-immunogenic [26,27]. Perfluoropropane is an inert gas, used as a constituent of commercially available echo contrast agents such as Optison and Definity [33], and is exhaled from the lungs [34]. Therefore, this echo contrast agent is generally considered nontoxic, although safety in humans remains to be demonstrated. Other potential barriers for clinical use are related to the specificity of the RGD peptide. This ligand is highly specific to activated platelet glycoprotein IIb/IIIa receptor [14,17]. However, the specificity is limited and this ligand may also bind to sites of angiogenesis, inflammation, osteoporosis and cancer [35]. In contrast, the relatively high specificity of this ligand to activated platelets may prevent the attachment of the targeted BL to organized chronic thrombi, although this hypothesis was not examined in the present experiment. Therefore, this agent may only enhance fresh thrombi on imaging and may provide a unique opportunity to distinguish fresh thrombi from old organized thrombi. Another limitation of this study is that we did not use the harmonic imaging technique, which is considered to improve ultrasound image quality, particularly when used with echo contrast agents. With the use of harmonic imaging, more distinct enhancement of thrombi can be expected in larger animals or humans.

In conclusion, perfluorocarbon gas-containing liposomal bubbles with RGD peptides are a novel echo contrast agent that can markedly enhance fresh thrombi on ultrasonic imaging *in vitro* and *in vivo*, and may be useful for noninvasive diagnosis of acute thrombotic vessel occlusion.

Acknowledgements

This study was supported in part by a Grant-in-Aid for Scientific Research (B) (16300176) from the Japan Society for the Promotion of Science and a Japan Heart Foundation Research Grant.

The authors of this manuscript have certified that they comply with the Principles of Ethical Publishing in the International Journal of Cardiology [36].

References

[1] Masses, tumors, and source of embolus. In: Feigenbaum H, Armstrong WF, Ryan T, editors. Feigenbaum's echocardiography. 6th ed. Philadelphia, PA: Lippincott Williams & Wilkins; 2005. p. 701–34.
[2] Rose SC, Zwiebel WJ, Murdock LE, et al. Insensitivity of color Doppler flow imaging for detection of acute calf deep venous thrombosis in asymptomatic postoperative patients. J Vasc Interv Radiol 1993;4:111–7.
[3] Popma JJ. Coronary arteriography and intravascular imaging. In: Libby P, Bonow RO, Mann DL, Zipes DP, editors. Braunwald's heart disease: a textbook of cardiovascular medicine. 8th ed. Philadelphia, PA: Saunders Elsevier; 2008. p. 495–6.
[4] Lanza GM, Wallace KD, Scott MJ, et al. A novel site-targeted ultrasonic contrast agent with broad biomedical application. Circulation 1996;94:3334–40.
[5] Unger EC, McCreery TP, Sweitzer RH, Shen D, Wu G. In vitro studies of a new thrombus-specific ultrasound contrast agent. Am J Cardiol 1998;81:58G–61G.
[6] Wu Y, Unger EC, McCreery TP, et al. Binding and lysing of blood clots using MRX-408. Invest Radiol 1998;33:880–5.
[7] Takeuchi M, Ogunyankin K, Pandian NG, et al. Enhanced visualization of intravascular and left atrial appendage thrombus with the use of a thrombus-targeting ultrasonographic contrast agent (MRX-408A1): in vivo experimental echocardiographic studies. J Am Soc Echocardiogr 1999;12:1015–21.
[8] Demos SM, Alkan-Onyuksel H, Kane BJ, et al. In vivo targeting of acoustically reflective liposomes for intravascular and transvascular ultrasonic enhancement. J Am Coll Cardiol 1999;33:867–75.
[9] Hamilton A, Huang SL, Warnick D, et al. Left ventricular thrombus enhancement after intravenous injection of echogenic immunoliposomes: studies in a new experimental model. Circulation 2002;105:2772–8.
[10] Alonso A, Della Martina A, Stroick M, et al. Molecular imaging of human thrombus with novel abciximab immunobubbles and ultrasound. Stroke 2007;38:1508–14.
[11] Suzuki R, Takizawa T, Negishi Y, et al. Gene delivery by combination of novel liposomal bubbles with perfluoropropane and ultrasound. J Control Release 2007;117:130–6.
[12] Suzuki R, Takizawa T, Negishi Y, et al. Tumor specific ultrasound enhanced gene transfer in vivo with novel liposomal bubbles. J Control Release 2008;125:137–44.
[13] Suzuki R, Takizawa T, Negishi Y, Utoguchi N, Maruyama K. Effective gene delivery with liposomal bubbles and ultrasound as novel non-viral system. J Drug Target 2007;15:531–7.
[14] Gyongyossy-Issa MIC, Muller W, Devine DV. The covalent coupling of Arg-Gly-Asp-containing peptides to liposomes: purification and biochemical function of the lipopeptide. Arch Biochem Biophys 1998;353:101–8.
[15] Nishiya T, Sloan S. Interaction of RGD liposomes with platelets. Biochem Biophys Res Commun 1996;224:242–5.
[16] Szoka Jr F, Papahadjopolus D. Procedure for preparation of liposomes with large internal aqueous space and high capture by reverse-phase evaporation. Proc Natl Sci U S A 1978;75:4194–8.
[17] Beer JH, Springer KT, Coller BS. Immobilized Arg-Gly-Asp (RGD) peptides of varying lengths as structural probes of the platelet glycoprotein IIb/IIIa receptor. Blood 1992;79:117–28.
[18] NIH image home page. http://rsb.info.nih.gov/nih-image/ Accessed January 29, 2010.
[19] Glauert AM, Lewis PR. Biological specimen preparation for transmission electron microscopy. In: Glauert AM, editor. Practical methods in electron microscopy Volume 17. London, UK: Portland Press; 1998.
[20] Steffen W, Fishbein MC, Luo H, et al. High intensity, low frequency catheter-delivered ultrasound dissolution of occlusive coronary artery thrombi: an in vitro and in vivo study. J Am Coll Cardiol 1994;24:1571–9.
[21] Nishioka T, Luo H, Fishbein MC, et al. Dissolution of thrombotic arterial occlusion by high intensity, low frequency ultrasound and dodecafluoropentane emulsion: an in vitro and in vivo study. J Am Coll Cardiol 1997;30:561–8.
[22] Lindner JR. Microbubbles in medical imaging: current applications and future directions. Nature Rev Drug Discov 2004;3:527–32.
[23] Lanza GM, Wickline SA. Targeted ultrasonic contrast agents for molecular imaging and therapy. Curr Probl Cardiol 2003;28:625–53.
[24] Klibanov AL, Maruyama K, Torchilin VP, Huang L. Amphipathic polyethyleneglycols effectively prolong the circulation time of liposomes. FEBS Lett 1990;268:235–7.
[25] Maruyama K, Yuda T, Okamoto A, Kojima S, Suginaka A, Iwatsuru M. Prolonged circulation time in vivo of large unilamellar liposomes composed of distearoyl phosphatidylcholine and cholesterol containing amphipathic poly(ethylene glycol). Biochim Biophys Acta 1992;1128:44–9.
[26] Lee TY, Lin CT, Kuo SY, Chang DK, Wu HC. Peptide-mediated targeting to tumor blood vessels of lung cancer for drug delivery. Cancer Res 2007;67:10958–65.
[27] Chang DK, Lin CT, Wu CH, Wu HC. A novel peptide enhances therapeutic efficacy of liposomal anticancer drugs in mice models of human lung cancer. PLoS ONE 2009;4:e4171.
[28] Storm G, Oussoren C, Peelers PAM, Barenholz Y. Tolerability of liposomes *in vivo*. In: Gregoriadis G, editor. Liposome technology. Boca Raton, FL: CRC Press, Inc.; 1993. p. 345–83.
[29] Davidson RN, Croft SL, Scott A, Maini M, Moody AH, Bryceson AD. Liposomal amphotericin B in drug-resistant visceral leishmaniasis. Lancet 1991;337:1061–2.
[30] Guaglianone P, Chan K, DelaFlor-Weiss E, et al. Phase I and pharmacologic study of liposomal daunorubicin (DaunoXome). Invest New Drugs 1994;12:103–10.
[31] Gabizon A, Peretz T, Sulkes A, et al. Systemic administration of doxorubicin-containing liposomes in cancer patients: a phase I study. Eur J Cancer Clin Oncol 1989;25:1795–803.
[32] Carpenter CP, Woodside MD, Kinkead ER, King JM, Sullivan LJ. Response of dogs to repeated intravenous injection of polyethylene glycol 4000 with notes on excretion and sensitization. Toxicol Appl Pharmacol 1971;18:35–40.
[33] Wei K, Mulvagh SL, Carson L, et al. The safety of Definity and Optison for ultrasound image enhancement: a retrospective analysis of 78, 383 administered contrast doses. J Am Soc Echocardiogr 2008;11:1202–6.
[34] Hutter JC, Luu HM, Mehlhaff PM, Killam AL, Dittrich HC. Physiologically based pharmacokinetic model for fluorocarbon elimination after the administration of an octafluoropropane-albumin microsphere sonographic contrast agent. J Ultrasound Med 1999;18:1–11.
[35] Meyer A, Auernheimer J, Modlinger A, Kessler H. Targeting RGD recognizing integrins: drug development, biomaterial research, tumor imaging and targeting. Curr Pharm Des 2006;12:2723–47.
[36] Coats AJ. Ethical authorship and publishing. Int J Cardiol 2009;131:149–50.

Journal of Controlled Release 156 (2011) 355–363

Contents lists available at ScienceDirect

Journal of Controlled Release

journal homepage: www.elsevier.com/locate/jconrel

GENE DELIVERY

Involvement of activated transcriptional process in efficient gene transfection using unmodified and mannose-modified bubble lipoplexes with ultrasound exposure

Keita Un [a,b], Shigeru Kawakami [a,*], Yuriko Higuchi [c], Ryo Suzuki [d], Kazuo Maruyama [d], Fumiyoshi Yamashita [a], Mitsuru Hashida [a,e,*]

[a] Department of Drug Delivery Research, Graduate School of Pharmaceutical Sciences, Kyoto University, 46-29 Yoshida-Shimoadachi-cho, Sakyo-ku, Kyoto 606-8501, Japan
[b] The Japan Society for the Promotion of Science (JSPS), Chiyoda-ku, Tokyo 102-8471, Japan
[c] Institute for Innovative NanoBio Drug Discovery and Development, Graduate School of Pharmaceutical Sciences, Kyoto University, 46-29 Yoshida-Shimoadachi-cho, Sakyo-ku, Kyoto 606-8501, Japan
[d] Department of Biopharmaceutics, School of Pharmaceutical Sciences, Teikyo University, 1091-1 Suwarashi, Midori-ku, Sagamihara, Kanagawa 252-5195, Japan
[e] Institute for Integrated Cell-Material Sciences (iCeMS), Kyoto University, Yoshida-Ushinomiya-cho, Sakyo-ku, Kyoto 606-8302, Japan

ARTICLE INFO

Article history:
Received 6 May 2011
Accepted 27 June 2011
Available online 3 July 2011

Keywords:
Gene transfection
Bubble lipoplex
Ultrasound
Transcription factor
Inflammatory response

ABSTRACT

Recently, our group developed ultrasound (US)-responsive and mannose-modified gene carriers (Man-PEG_{2000} bubble lipoplexes), and successfully obtained a high level of gene expression in mannose receptor-expressing cells following gene transfection using Man-PEG_{2000} bubble lipoplexes and US exposure. We also reported that large amounts of plasmid DNA (pDNA) were transferred into the cytoplasm of the targeted cells in the gene transfection using this method. In the present study, we investigated the involvement of transcriptional processes on enhanced gene expression obtained by unmodified and Man-PEG_{2000} bubble lipoplexes with US exposure. The transcriptional process related to activator protein-1 (AP-1) and nuclear factor-κB (NFκB) was activated by US exposure, and was founded to be involved in enhanced gene expression obtained by gene transfection using unmodified and Man-PEG_{2000} bubble lipoplexes with US exposure. On the other hand, activation of AP-1 and NFκB pathways followed by US exposure was hardly involved in the inflammatory responses in the gene transfection using this method. These findings suggest that activation of AP-1 and NFκB followed by US exposure is involved in the enhanced gene expression using unmodified and Man-PEG_{2000} bubble lipoplexes with US exposure, and the selection of pDNAs activated by US exposure is important in this gene transfection method.

© 2011 Elsevier B.V. All rights reserved.

1. Introduction

Various obstacles are associated with in vivo gene transfection, including the control of in vivo distribution of nucleic acids, the improvement of intracellular/intranuclear transport of nucleic acids, and the activation of transcriptional/translational processes directly involved in the gene expression [1,2]. Viral and non-viral carriers have been studied as valuable gene carriers for in vivo gene transfection [3–6], with both possessing advantages and disadvantages relating to safety, productivity and gene expressing efficiency. Hama and Harashima et al. have reported that the high gene expression efficiency in gene transfection using viral carrier is influenced by the high transcriptional and translational efficiency following intranuclear transport of pDNA [7,8]. Therefore, the transcriptional/translational processes associated with gene transfection of non-viral carriers are potentially controlled by improved gene expression efficiency.

Gene transfection methods using physical stimulation, such as electroporation method [9], hydrodynamic injection [10,11], tissue pressure-mediated method [12] and sonoporation method [13], enable to obtain high-level gene expression. Gene expression has also been reported to be enhanced by intracytoplasmic transfer of pDNA as a result of using these methods [14–16]. Recently, our group developed US-responsive and/or mannose-modified gene carriers (unmodified and Man-PEG_{2000} bubble lipoplexes), and reported that high level gene expression can be selectively obtained in mannose receptor-expressing cells following intravenous administration of Man-PEG_{2000} bubble lipoplexes and US exposure, both in vitro and in vivo [17,18]. Furthermore, we have reported that large amounts of pDNA are transferred into the cytoplasm of targeted cells in the gene transfection using unmodified and Man-PEG_{2000} bubble lipoplexes with optimized US exposure under both in vitro and in vivo conditions [19].

Various types of physical stimulations, such as electric pulse, physical pressure, radiation and US exposure, can activate the transcriptional process involved in the AP-1-mediated and NFκB-

* Corresponding authors. Tel.: +81 75 753 4545; fax: +81 75 753 4575.
E-mail addresses: kawakami@pharm.kyoto-u.ac.jp (S. Kawakami), hashidam@pharm.kyoto-u.ac.jp (M. Hashida).

0168-3659/$ – see front matter © 2011 Elsevier B.V. All rights reserved.
doi:10.1016/j.jconrel.2011.06.040

mediated pathways [20–26]. It has been reported that this activation of transcription followed by physical stimulation partly contributes to the high gene expression observed when using the hydrodynamics and physical pressure-mediated methods [21,22,27]. However, there are few reports that the transcriptional process is activated by US exposure in vivo. Moreover, there is little information that the transcriptional activation followed by US exposure involves in the enhanced gene expression by in vitro and in vivo gene transfection using sonoporation method.

Our present study investigated the involvement of transcriptional processes in enhanced gene expression obtained by transfection using unmodified and Man-PEG_{2000} bubble lipoplexes with US exposure. We examined the gene transfection efficiency obtained by US-mediated gene transfection using pDNAs controlled by various transcription factors including AP-1, NFκB, cyclic adenosine 3′,5′-monophosphate response element (CRE) and serum response element (SRE), in RAW264.7 cell lines, primary mouse cultured macrophages, and mice. Then, we evaluated the gene expression and intranuclear transport of transcription factors, such as AP-1 [28] and NFκB [29,30], followed by gene transfection using unmodified and Man-PEG_{2000} bubble lipoplexes with US exposure, both in vitro and in vivo. Finally, the involvement of activated transcription on inflammatory cytokine production was also examined, since activation of specific transcriptional factors might contribute to the inflammatory responses [31,32].

2. Materials and methods

2.1. Materials

1,2-Distearoyl-*sn*-glycero-3-trimethylammoniumpropane (DSTAP), 1,2-distearoyl-*sn*-glycero-3-phosphocholine (DSPC) and 1,2-distearoyl-*sn*-glycero-3-phosphoethanolamine-N-[amino (polyethylene glycol)-2000] (NH_2-PEG_{2000}-DSPE) were purchased from Avanti Polar Lipids (Alabaster, AL, USA), Sigma-Aldrich (St. Louis, MO, USA) and NOF (Tokyo, Japan), respectively. RPMI-1640 was purchased from Nissui Pharmaceutical (Tokyo, Japan) and fetal bovine serum (FBS) was purchased from Japan Bioserum (Hiroshima, Japan). All other chemicals were of the highest purity available.

2.2. pDNA, cell lines and mice

pCMV-Luc was constructed as described previously [33]. Briefly, the HindIII/Xba I firefly luciferase cDNA fragment from pGL3-control vector (Promega, Madison, WI, USA) was sub-cloned into the polylinker of pcDNA3 vector (Invitrogen, Carlsbad, CA, USA). Pathway profiling luciferase systems (pTA/Luc, pAP-1/Luc, pNFκB/Luc, pCRE/Luc and pSRE/Luc) were purchased from Clontech Laboratories (Mountain View, CA, USA). pDNA was amplified in the *Escherichia coli* strain DH5α, isolated and purified using a QIAGEN Endofree Plasmid Giga Kit (QIAGEN, Hilden, Germany). RAW264.7 cells, from a murine macrophage-like cell line, were cultured in RPMI-1640 supplemented with 10% FBS, 100 IU/ml penicillin, 100 μg/ml streptomycin, and 2 mM L-glutamine. Cells were plated onto 24-well culture plates at a density of 5×10^4 cells/1.88 cm^2 at 37 °C in 5% CO_2, and incubated for 48 h prior to experiments. Female ICR mice (4-week-old) and female C57BL/6 mice (6-week-old) were purchased from Japan SLC (Shizuoka, Japan). All animal experiments were carried out in accordance with the Principles of Laboratory Animal Care, as adopted and propagated by the U.S. National Institutes of Health and the Kyoto University Guidelines for Animal Experiments.

2.3. Construction of Man-PEG_{2000} bubble lipoplexes

Man-PEG_{2000} bubble lipoplexes were constructed according to our previous report [17]. Briefly, DSTAP, DSPC, and NH_2-PEG_{2000}-DSPE or mannose-modified PEG_{2000}-DSPE were mixed in chloroform at a molar ratio of 7:2:1 to produce the liposomes for bubble lipoplexes. The liposome construction mixture was dried by evaporation and vacuum desiccated before the resultant lipid film was resuspended in sterile 5% dextrose. After hydration for 30 min at 65 °C, the dispersion was sonicated for 10 min in a bath sonicator and 3 min in a tip sonicator for liposome production. Liposomes were then sterilized by passage through a 0.45 μm filter (PALL, East Hills, NY, USA). Lipoplexes were prepared by gently mixing with equal volumes of pDNA and liposome solution at a charge ratio of 1.0:2.3 (−:+). Prepared lipoplexes were pressurized with perfluoropropane gas (Takachiho Chemical Industries, Tokyo, Japan) and sonicated using a bath-type sonicator (AS ONE, Osaka, Japan) for 5 min to enclose US imaging gas. Particle sizes and ζ-potentials of the liposomes/lipoplexes were determined using a Zetasizer Nano ZS instrument (Malvern Instrument, Worcestershire, UK).

2.4. Harvesting of mouse peritoneal macrophages

Mouse peritoneal macrophages were harvested and cultured as previously described [34]. Briefly, the macrophages were harvested from the peritoneal cavity of female ICR mice, before being washed and suspended in RPMI-1640 medium supplemented with 10% FBS, 100 IU/ml penicillin, 100 μg/ml streptomycin and 2 mM L-glutamine, and plated onto 24-well culture plates at a density of 2×10^5 cells/1.88 cm^2. After incubation for 2 h at 37 °C in 5% CO_2, non-adherent cells were washed off with culture medium, and the macrophages were incubated for another 72 h.

2.5. In vitro gene transfection

After RAW264.7 cells and macrophages were plated and incubated for 48 and 72 h, respectively, the culture medium was replaced with Opti-MEM I containing bubble lipoplexes (5 μg pDNA). Cells were exposed to US (frequency, 2.062 MHz; duty, 50%; burst rate, 10 Hz; intensity 4.0 W/cm^2) for 20 s using a Sonopore-4000 sonicator (NEPA GENE, Chiba, Japan) with a 6 mm diameter probe placed in each well at predetermined times after the addition of bubble lipoplexes. At 1 h after addition of bubble lipoplexes, the incubation medium was replaced with RPMI-1640 and incubated for an additional time. Subsequently, the cells were scraped from the plates and suspended in lysis buffer (0.05% Triton X-100, 2 mM EDTA, 0.1 M Tris, pH 7.8). The cell suspension was shaken, and centrifuged at 10,000×*g*, 4 °C for 10 min. Luciferase assay buffer (Picagene; Toyo Ink, Tokyo, Japan) was mixed with the supernatant and the luciferase activity was measured in a luminometer (Lumat LB 9507; EG&G Berthold, Bad Wildbad, Germany). Luciferase activity was normalized against the cellular protein content. Protein concentration was determined with a Protein Quantification Kit (Dojindo Molecular Technologies, Tokyo, Japan).

2.6. In vivo gene transfection

Mice were intravenously injected with 400 μl of bubble lipoplexes via the tail vein using a 26-gauge syringe needle at a dose of 50 μg pDNA. At predetermined times after the injection, US (frequency, 1.045 MHz; duty, 50%; burst rate, 10 Hz; intensity 1.0 W/cm^2; time, 2 min) was exposed transdermally to the abdominal area using a Sonopore-4000 sonicator (NEPA GENE) with a 20 mm diameter probe. At predetermined times after injection, mice were sacrificed and organs were collected for each experiment. Organs were washed twice with cold saline and homogenized with lysis buffer (0.05% Triton X-100, 2 mM EDTA, 0.1 M Tris, pH 7.8). Lysis buffer was added at a weight ratio of 5 ml/g for the liver or 4 ml/g for other organs. After 3 cycles of freezing and thawing, the homogenates were centrifuged at 10,000×*g* at 4 °C for 10 min. Luciferase activity of the resulting supernatant was determined by above-mentioned luciferase assay.

2.7. Quantitative reverse transcription-polymerase chain reaction (RT-PCR)

Total ribonucleic acid (RNA) was isolated from the cells and organs using a GenElute Mammalian Total RNA Miniprep Kit (Sigma-Aldrich). Reverse transcription of messenger RNA (mRNA) was carried out using PrimeScript® RT reagent Kit (Takara Bio, Shiga, Japan). The detection of complementary deoxyribonucleic acid (cDNA) (*c-fos*, *c-jun*, *p105*, *p65* and *gapdh*) was conducted using real-time PCR using SYBR® Premix Ex Taq (Takara Bio) and a Lightcycler Quick System 350S (Roche Diagnostics, Indianapolis, IN, USA). Primers for *c-fos*, *c-jun*, *p105*, *p65* and *gapdh* cDNA were synthesized by Sigma-Aldrich as follows: *c-fos*, 5′-CCA GTC AAG AGC ATC AGC AA-3′ (forward) and 5′-AAG TAG TGC AGC CCG GAG TA-3′ (reverse); *c-jun*, 5′-TCC CCT ATC GAC ATG GAG TC-3′ (forward) and 5′-TGA GTT GGC ACC CAC TGT TA-3′ (reverse); *p105*, 5′-CCT GGA TGA CTC TTG GGA AA-3′ (forward) and 5′-TCA GCC AGC TGT TTC ATG TC-3′ (reverse); *p65*, 5′-TAG CAC CTG ATG GCT GAC TG-3′ (forward) and 5′-CGT TCC ACC ACA TCT GTG TC-3′ (reverse); *gapdh*, 5′-TCT CCT GCG ACT TCA ACA-3′ (forward) and 5′-GCT GTA GCC GTA TTC ATT GT-3′ (reverse). mRNA copy number was calculated for each sample from the standard curve using the thermal-cycler software ('Arithmetic Fit Point analysis' for the Lightcycler). Results were expressed as relative copy number calculated relative to *gapdh* mRNA (*c-fos*, *c-jun*, *p105*, *p65* mRNA copy number/*gapdh* mRNA copy number).

2.8. Measurement of the level of intranuclear protein

Cells and tissues were collected at predetermined times after gene transfection, and the nuclear extract from cells and tissues was prepared using a Nuclear Extract Kit (Active Motif, Carlsbad, CA, USA). Nuclear protein was divided into aliquots and stored at −80 °C for later use. The protein concentration was measured with a Protein Quantification Kit. The amounts of p50 and p65, which are the components of NFκB in the cellular nuclear extract was measured using a NFκB (p50) Transcription Factor Kit (Thermo Fisher Scientific, Waltham, MA, USA) and a NFκB (p65) transcription Factor Assay Kit (Cayman Chemical, Ann Arbor, MI, USA), respectively, according to the manufacturer's protocols.

2.9. Measurement of inflammatory cytokines

At predetermined times after the in vitro and in vivo gene transfection, the supernatants and serum were collected and the cytokine levels (TNF-α, IFN-γ, and IL-6) were determined with a commercial enzyme-linked immunosorbent assay (ELISA) Kit (Bay Bioscience, Hyogo, Japan) according to the recommended procedures.

2.10. Statistical analysis

Results were presented as the mean ± S.D. of more than three experiments. Analysis of variance (ANOVA) was used to test the statistical significance of differences among groups. Two-group comparisons were performed by Student's *t*-test. Multiple comparisons between control and test groups were performed by Dunnett's test and multiple comparisons between all groups were performed using the Tukey–Kramer test.

3. Results

3.1. Physicochemical properties of lipoplexes and bubble lipoplexes used in this study

The physicochemical properties of lipoplexes and bubble lipoplexes constructed with various pDNAs used in all experiments were evaluated by measuring the particle sizes and ζ-potentials. Mean particle sizes and ζ-potentials of unmodified and Man-PEG_{2000} lipoplexes were approximately 137 nm and +48 mV, respectively (Supplementary Table 1). Moreover, mean particle sizes and ζ-potentials of unmodified and Man-PEG_{2000} bubble lipoplexes were approximately 550 nm and +48 mV, respectively (Supplementary Table 1). These results correspond to previous reports [17–19]; suggesting that these pDNA had no effect on the physicochemical properties of lipoplexes and bubble lipoplexes.

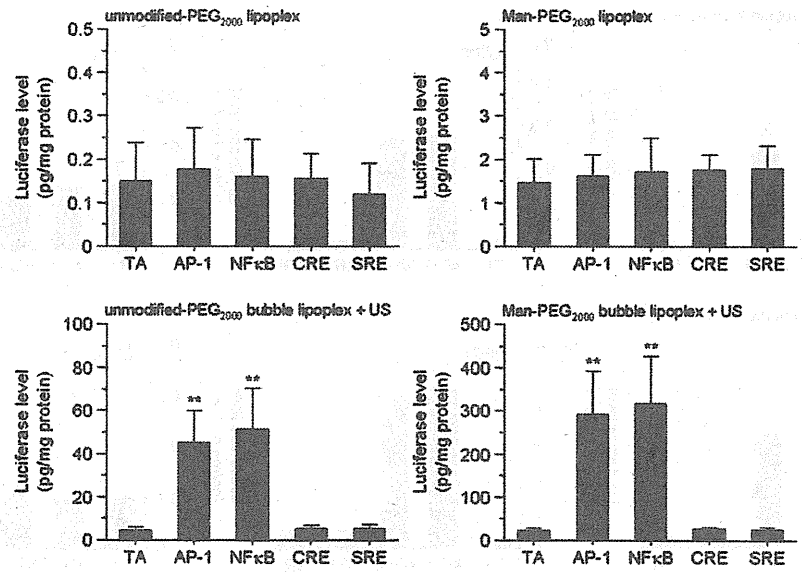

Fig. 1. The effect of transcriptional factors on gene expression obtained by unmodified and Man-PEG_{2000} bubble lipoplexes with or without US exposure in mouse cultured macrophages. Luciferase expression levels obtained by unmodified-PEG_{2000} lipoplexes, Man-PEG_{2000} lipoplexes, unmodified-PEG_{2000} bubble lipoplexes with US exposure, and Man-PEG_{2000} bubble lipoplexes with US exposure (5 μg of pDNA) at 24 h after transfection in mouse primary cultured macrophages. Lipoplexes were constructed with pDNAs controlled by various transcription factors. Each value represents the mean + S.D. ($n = 4$). Key: TA; pTA/Luc, AP-1; pAP-1/Luc, NFκB; pNFκB/Luc, CRE; pCRE/Luc, SRE; pSRE/Luc. $^{**}p < 0.01$, compared with the corresponding TA group.

3.2. Involvement of transcriptional process on enhanced gene expression obtained by unmodified and Man-PEG$_{2000}$ bubble lipoplexes with US exposure in vitro

The involvement of transcription on enhanced gene expression obtained by unmodified and Man-PEG$_{2000}$ bubble lipoplexes with US exposure was investigated in mouse primary cultured macrophages. First, we examined gene expression levels using unmodified/Man-PEG$_{2000}$ lipoplexes or bubble lipoplexes constructed with luciferase expressing-pDNA controlled by various transcription factors, including AP-1, NFκB, CRE and SRE. Gene expression levels obtained by Man-PEG$_{2000}$ lipoplexes only or Man-PEG$_{2000}$ bubble lipoplexes with US exposure were higher than those by unmodified-PEG$_{2000}$ formulations (Fig. 1), since mouse cultured macrophages express the mannose receptors abundantly. Moreover, although the level of gene expression obtained by both lipoplexes was similar in all pDNAs, the level of gene expression obtained by both bubble lipoplexes and US exposure was enhanced approximately 10-fold by gene transfection using pAP-1/Luc and pNFκB/Luc, compared with that using pTA/Luc, which is a pDNA without transcription factor-binding site within the enhancer region (Fig. 1). Similar results were observed in the murine macrophage-like RAW264.7 cells (Supplementary Fig. 1).

3.3. Involvement of transcriptional process on enhanced gene expression obtained by unmodified and Man-PEG$_{2000}$ bubble lipoplexes with US exposure in mice

Next, we investigated the level of gene expression by in vivo gene transfection using unmodified/Man-PEG$_{2000}$ lipoplexes and bubble lipoplexes constructed with luciferase expressing-pDNA controlled by

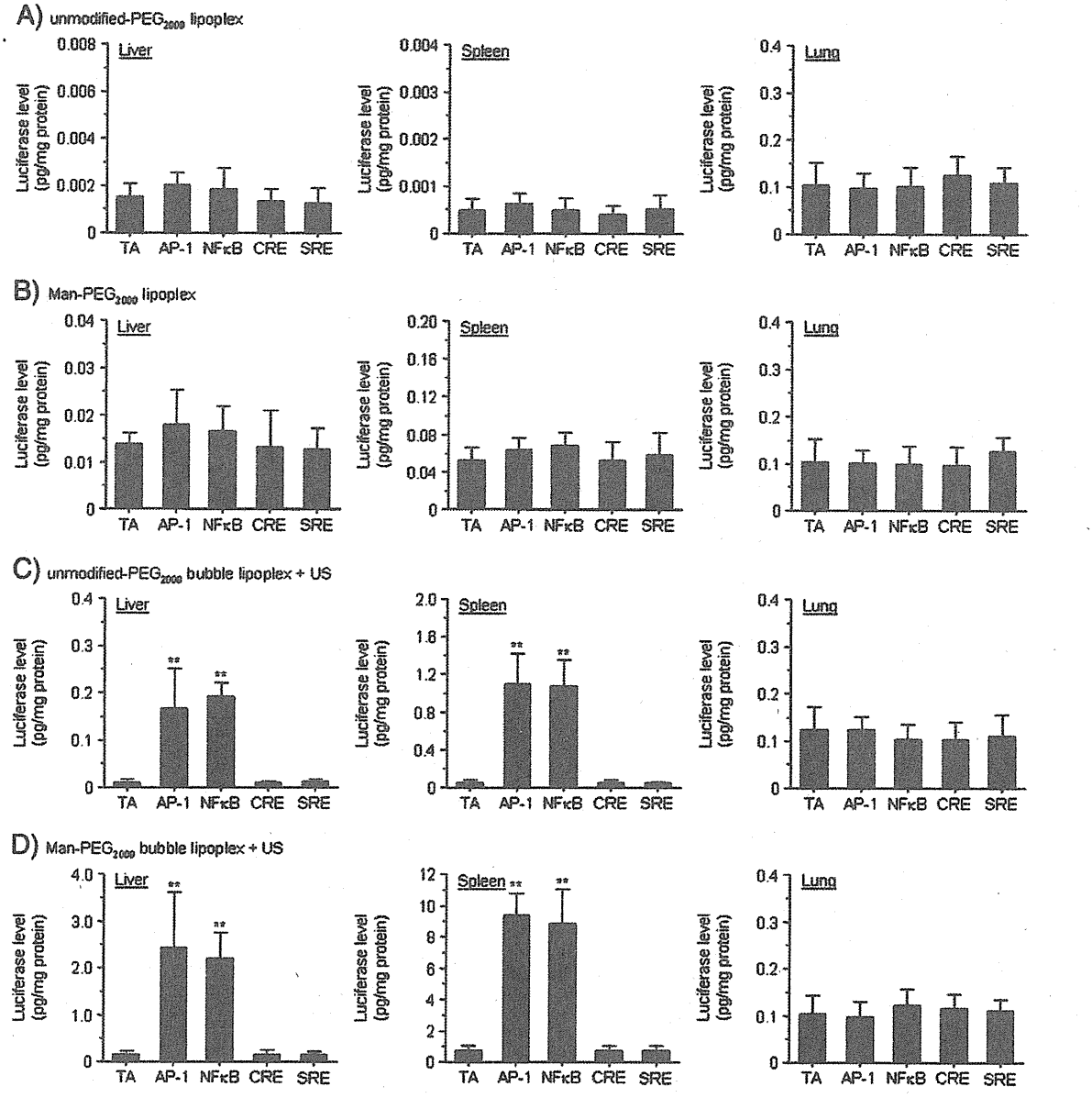

Fig. 2. The effect of transcriptional factors on gene expression obtained by unmodified and Man-PEG$_{2000}$ bubble lipoplexes with or without US exposure in vivo. Luciferase expression levels obtained by unmodified-PEG$_{2000}$ lipoplexes (A), Man-PEG$_{2000}$ lipoplexes (B), unmodified-PEG$_{2000}$ bubble lipoplexes with US exposure (C), and Man-PEG$_{2000}$ bubble lipoplexes with US exposure (D) (50 μg of pDNA) in the liver, spleen and lung at 6 h after transfection. Lipoplexes were constructed with pDNAs controlled by various types of transcriptional factors. Each value represents the mean + S.D. ($n=4$). Key: TA; pTA/Luc, AP-1; pAP-1/Luc, NFκB; pNFκB/Luc, CRE; pCRE/Luc, SRE; pSRE/Luc. $^{**}p<0.01$, compared with the corresponding TA group.

various transcription factors. Gene expression levels in the liver and spleen obtained by Man-PEG_{2000} lipoplexes only or Man-PEG_{2000} bubble lipoplexes with US exposure were higher than those by unmodified-PEG_{2000} formulations (Fig. 2), since liver and spleen are the major target organ of mannose-modified carriers. Although the level of gene expression obtained by both lipoplexes was similar in all pDNAs (Fig. 2A and B), gene expression levels in the liver and spleen obtained by both bubble lipoplexes and US exposure were enhanced approximately 10-fold by gene transfection using pAP-1/Luc and pNFκB/Luc, compared with that using pTA/Luc (Fig. 2C and D). On the other hand, enhanced gene expression followed by gene transfection using bubble lipoplexes constructed with pAP-1/Luc or pNFκB/Luc was not observed in the lung.

3.4. The effect of in vitro gene transfection using unmodified and Man-PEG_{2000} bubble lipoplexes with US exposure on AP-1 and NFκB

Following examination of the expression properties for c-fos and c-jun, which are the components of AP-1, *c-fos* and *c-jun* mRNA expression was enhanced transiently in mouse primary cultured macrophages by not only the gene transfection using bubble lipoplexes and US exposure, but also US exposure alone (Fig. 3A). Moreover, enhanced expression of *c-fos* and *c-jun* mRNA was not observed in the gene transfection using lipoplexes only (Fig. 3A). Evaluation of the expressing properties and intranuclear transporting properties of NFκB followed by gene transfection revealed that *p105* (precursor of p50) and *p65* mRNA expression in mouse primary cultured macrophages was not enhanced in all of groups, which differed from the results obtained for *c-fos* and *c-jun* mRNA (Supplementary Fig. 2). In contrast, the amount of intranuclear p50 and p65 increased transiently by not only the gene transfection using bubble lipoplexes and US exposure, but also US exposure alone (Fig. 3B). On the other hand, enhanced intranuclear transport of p50 and p65 was not observed in the gene transfection using lipoplexes only (Fig. 3B). Moreover, these transient AP-1 expression and intranuclear transport of NFκB followed by US exposure were also observed in RAW264.7 cells in this gene transfection method (Supplementary Fig. 3). These results suggest that transcription activation, such as increased AP-1 expression and enhanced intranuclear transport of NFκB, is partly involved in enhanced gene expression produced by unmodified and Man-PEG_{2000} bubble lipoplexes with US exposure.

3.5. The effect of in vivo gene transfection using unmodified and Man-PEG_{2000} bubble lipoplexes with US exposure on AP-1 and NFκB

c-fos/c-jun mRNA expression and the intranuclear amount of p50/p65 were enhanced transiently by not only the gene transfection using bubble lipoplexes and US exposure, but also US exposure alone in both the liver and spleen (Figs. 4 and 5). On the other hand, these phenomena were not observed in the lung (Figs. 4C and 5C). In addition, *c-fos* and *c-jun* mRNA expression levels in the liver and spleen followed by US exposure were dependedent on the US intensity (Supplementary Fig. 4).

3.6. The effect of in vitro and in vivo gene transfection using unmodified and Man-PEG_{2000} bubble lipoplexes and US exposure on inflammatory cytokine production

Increased AP-1 expression and intranuclear transport of NFκB followed by US exposure were demonstrated to be involved in the enhanced gene expression by unmodified and Man-PEG_{2000} bubble lipoplexes with US exposure. On the other hand, since these phenomena are potentially involved in the production of inflammatory cytokines [31,32], the production properties of inflammatory cytokines followed by gene transfection were investigated in vitro and in vivo. Although TNF-αproduction followed by gene transfection using only lipoplexes was significantly increased time-dependently in RAW264.7 cells and mouse primary cultured macrophages, only a slight increase in TNF-α production was observed followed by gene transfection using bubble lipoplexes and US exposure (Fig. 6).

While the inflammatory cytokines (TNF-α, IFN-γ, and IL-6) in the serum followed by in vivo gene transfection exhibited transient and significant increases in all of gene transfection methods (Fig. 7), the

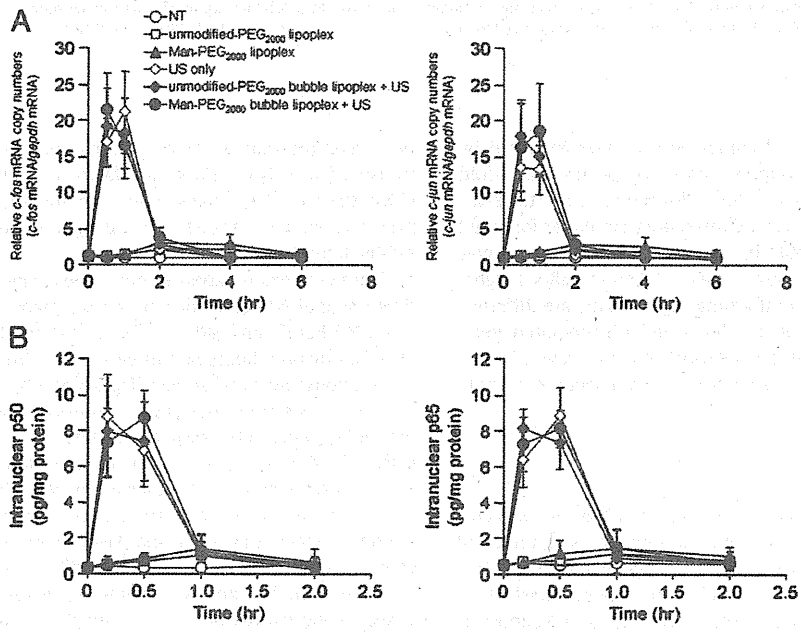

Fig. 3. Enhanced *c-fos/c-jun* mRNA expression and intranuclear transport of p105/p65 followed by gene transfection using unmodified and Man-PEG_{2000} bubble lipoplexes with or without US exposure in mouse primary cultured macrophages. Time-course of *c-fos/c-jun* mRNA expression levels (A) and intranuclear p105/p65 levels (B) followed by various transfection methods (5 μg of pCMV-Luc) in mouse primary cultured macrophages. Each value represents the mean ± S.D. ($n=4$). $^{**}p<0.01$, compared with the corresponding non-treatment (NT) group.

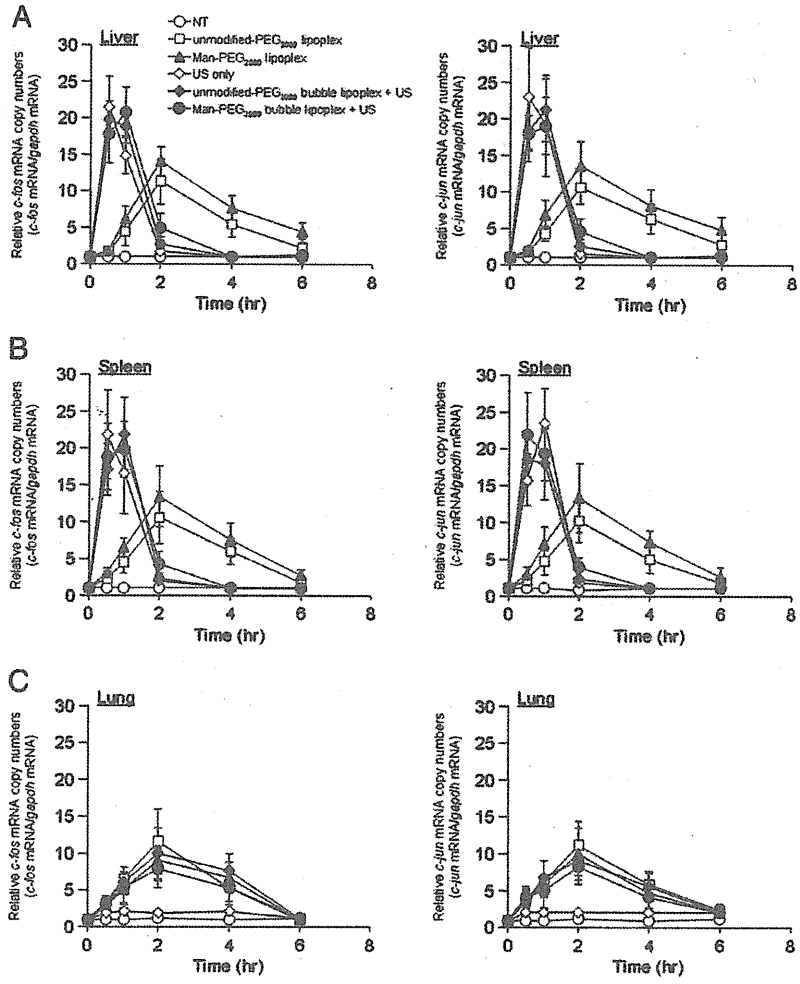

Fig. 4. Enhanced *c-fos/c-jun* mRNA expression followed by gene transfection using unmodified and Man-PEG_{2000} bubble lipoplexes with or without US exposure in vivo. Time-course of *c-fos* and *c-jun* mRNA expression levels in the liver (A), spleen (B), and lung (C) followed by various transfection methods (50 μg of pCMV-Luc) in mice. Each value represents the mean ± S.D. ($n = 4$). NT; non-treatment.

maximum amount of secreted inflammatory cytokines followed by gene transfection using bubble lipoplexes and US exposure was 3-fold lower than that using lipoplexes only. Moreover, the time-to-maximum concentration of secreted inflammatory cytokines followed by gene transfection using bubble lipoplexes and US exposure was earlier than that using only lipoplexes (Fig. 7). These results suggest that the production properties of inflammatory cytokine are different between conventional lipofection methods and US-mediated gene transfection methods, and that inflammatory cytokines have a minor effect on enhanced AP-1 expression/NFκB intranuclear transport followed by US exposure.

4. Discussion

We recently reported that large amounts of pDNA are directly transferred into the cytoplasm in the gene transfection using unmodified and Man-PEG_{2000} bubble lipoplexes with US exposure [17,19]. However, this enhanced gene expression followed by gene transfection using unmodified and Man-PEG_{2000} bubble lipoplexes with US exposure may not correspond to the increase of intracellular pDNA by targeted delivery of pDNA and intracytoplasmic transfer of pDNA; suggesting the involvement of the other factors on the enhanced gene expression in the gene transfection using both bubble lipoplexes and US exposure. It has been reported that the transcriptional process following intranuclear transport of pDNA is important factor in gene transfection efficiency [7,8]; therefore, we investigated the involvement of transcriptional processes in gene transfection using unmodified and Man-PEG_{2000} bubble lipoplexes with US exposure.

Following examination of gene expression levels using luciferase-expressing pDNAs controlled by various transcription factors, including AP-1, NFκB, CRE and SRE, we found that the level of gene expression obtained by both lipoplexes in vitro (Fig. 1 and Supplementary Fig. 1), and in mouse liver and spleen (Fig. 2A and B), was similar in all pDNAs studied. On the other hand, gene expression levels using pAP-1/Luc and pNFκB/Luc were approximately 10-fold higher than those using other pDNAs in the gene transfection using unmodified and Man-PEG_{2000} bubble lipoplexes with US exposure in vitro (Fig. 1 and Supplementary Fig. 1), and in mouse liver and spleen (Fig. 2C and D). These results strongly suggest that AP-1 and NFκB were involved in the enhanced gene expression obtained by unmodified and Man-PEG_{2000} bubble lipoplexes with US exposure. Therefore, we further investigated the AP-1/NFκB gene expression and intranuclear transport followed by this gene transfection method.

c-fos/c-jun mRNA expression (Figs. 3A and 4) and intranuclear p50/p65 levels (Figs. 3B and 5) were enhanced transiently by not only the gene transfection using both bubble lipoplexes and US exposure,

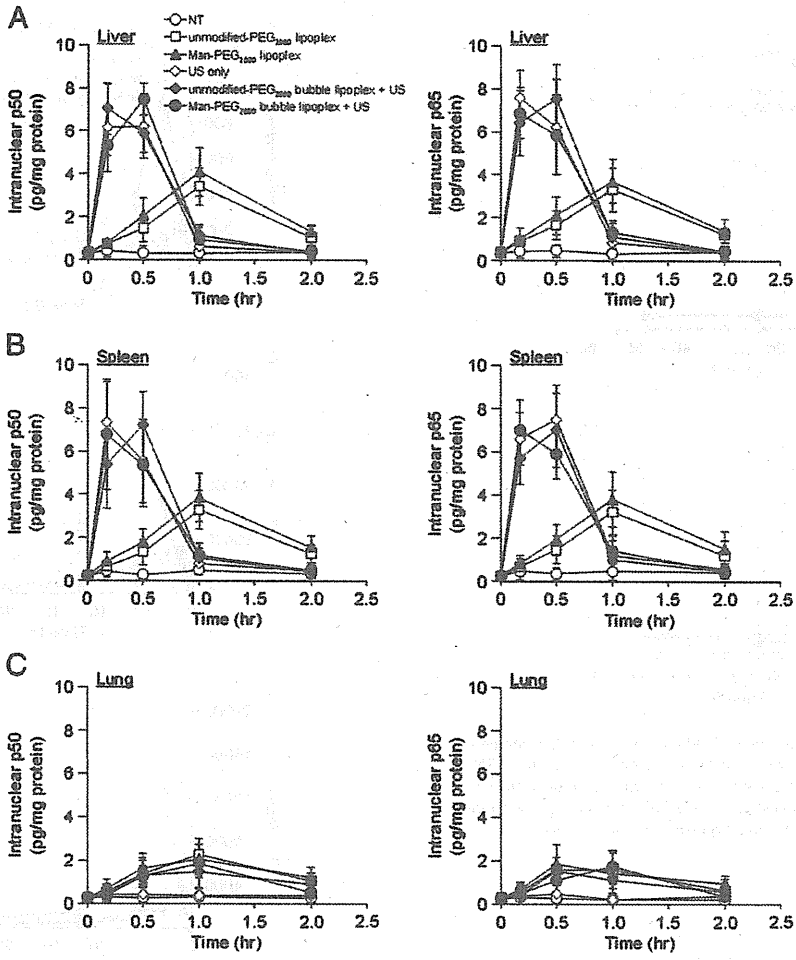

Fig. 5. Enhanced intranuclear transport of p50 and p65 followed by gene transfection using unmodified and Man-PEG_{2000} bubble lipoplexes with or without US exposure in vivo. Time-course of intranuclear p50 and p65 levels in the liver (A), spleen (B), and lung (C) followed by various transfection methods (50 μg of pCMV-Luc) in mice. Each value represents the mean ± S.D. ($n = 3$). NT; non-treatment.

but also US exposure alone in vitro, and in mouse liver and spleen. It has been reported that US exposure induced the enhanced expression of c-fos and c-jun via phosphorylation of ERK, p38 and JNK [25,26], and our results partially correspond to these reports. These observations led us to believe that the activation of AP-1 and NFκB-mediated transcriptional processes followed by US exposure is involved in the enhanced gene expression using unmodified and Man-PEG_{2000} bubble lipoplexes with US exposure.

Since the activation of transcription factors such as AP-1 [28] and NFκB [29,30] is involved in the induction of inflammatory responses [31,32], we investigated the production properties of inflammatory cytokines followed by this gene transfection method. The production levels of TNF-α, IFN-γ or IL-6 followed by gene transfection using both bubble lipoplexes and US exposure were substantially lower than that using both lipoplexes in vitro (Fig. 6) and in vivo (Fig. 7). We previously reported that the inflammatory responses were significantly suppressed in the gene transfection method using unmodified and Man-PEG_{2000} bubble lipoplexes with US exposure, because a large amount of pDNA was transferred into the cytoplasm directly through the transient pores created by the destruction of both bubble lipoplexes followed by US exposure [19], suggesting that pDNA is hardly interacted with endosomal TLR-9. On the other hand, it was reported that the phosphorylation of AP-1 and NFκB was induced via the activation of p38, ERK and JNK-mediated pathways followed by US exposure [25,26], and we showed that these AP-1 and NFκB activation was transiently in our sonoporation method and condition in this study (Figs. 3–5 and Supplementary Fig. 3). Although these activation of AP-1 and NFκB leads to the inflammatory cytokine production [31,32], the inflammatory responses induced by AP-1 and NFκB activation followed by US exposure were low under in vitro and in vivo condition (Figs. 6 and 7). We previously have reported that the activating level of transcriptional factors, such as c-fos and c-jun, in tissue pressure-mediated transfection method was approximately one-fifth, compared with that in hydrodynamics method [22]. Moreover, the production of inflammatory cytokines under in vivo condition followed by tissue pressure-mediated transfection method was much lower than those by conventional lipofection method [35]. The activating levels of transcriptional factors followed by our sonoporation method using unmodified and Man-PEG_{2000} bubble lipoplexes with US exposure were almost the same with that by tissue pressure-mediated transfection method. Therefore, the contribution of the inflammatory response induced by AP-1 and NFκB activation followed by our sonoporation method may be negligible. These results suggest that the transient expression of AP-1 and the transient intranuclear transport of NFκB followed by US exposure might be minimally involved in the inflammatory responses in the gene transfection using unmodified and Man-PEG_{2000} bubble lipoplexes with US exposure.

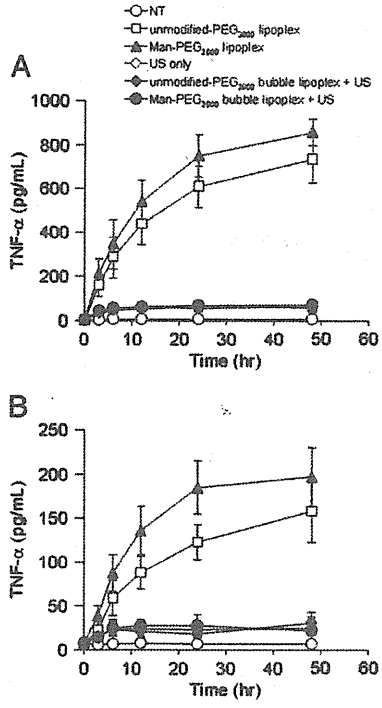

Fig. 6. Evaluation of TNF-α secretion followed by gene transfection using unmodified and Man-PEG_{2000} bubble lipoplexes with or without US exposure in vitro. TNF-α concentration in the supernatant was measured following various transfection methods (5 μg of pDNA) at predetermined times in RAW264.7 cells (A) and mouse primary cultured macrophages (B). Each value represents the mean ± S.D. ($n = 4$).

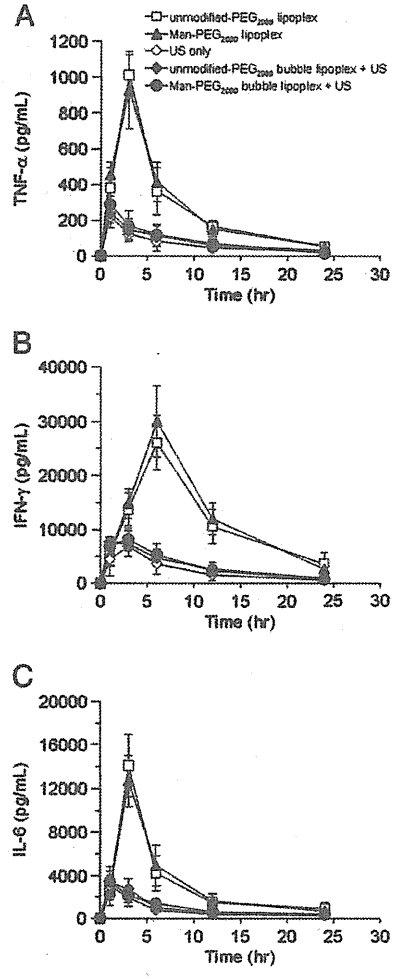

Fig. 7. Evaluation of pro-inflammatory cytokine secretion in serum followed by gene transfection using unmodified and Man-PEG_{2000} bubble lipoplexes with or without US exposure in vivo. TNF-α (A), IFN-γ (B), and IL-6 (C) concentrations in the serum were measured following various transfection methods (50 μg of pDNA) at predetermined times in mice. Each value represents the mean ± S.D. ($n = 4$).

5. Conclusion

Our results suggest that the activated AP-1 and NFκB followed by US exposure is involved in the enhanced gene expression using unmodified and Man-PEG_{2000} bubble lipoplexes with US exposure. These results suggest that enhanced gene expression in the gene transfection using our sonoporation method was obtained by applying pDNA controlled by the specific transcriptional factors. Therefore, the selection of suitable pDNA with specific promoter regions activated by US stimulation is one of the important factors for efficient gene expression in our gene transfection method. In addition, the transient expression of AP-1 and the transient intranuclear transport of NFκB followed by US exposure were not substantially involved in the inflammatory responses in this gene transfection method. These findings may help in the development of an effective gene transfection method using US-exposing system.

Acknowledgments

This work was supported in part by a Grant-in-Aid for Young Scientists (A) from the Ministry of Education, Culture, Sports, Science and Technology of Japan, and by Health and Labour Sciences Research Grants for Research on Noninvasive and Minimally Invasive Medical Devices from the Ministry of Health, Labour and Welfare of Japan, and by the Programs for Promotion of Fundamental Studies in Health Sciences of the National Institute of Biomedical Innovation (NIBIO).

Appendix A. Supplementary data

Supplementary data to this article can be found online at doi:10.1016/j.jconrel.2011.06.040.

References

[1] M. Thomas, A.M. Klibanov, Non-viral gene therapy: polycation-mediated DNA delivery, Appl. Microbiol. Biotechnol. 2003 (2003) 27–34.
[2] T. Ito, N. Iida-Tanaka, T. Niidome, T. Kawano, K. Kubo, K. Yoshikawa, T. Sato, Z. Yang, Y. Koyama, Hyaluronic acid and its derivative as a multi-functional gene expression enhancer: protection from non-specific interactions, adhesion to targeted cells, and transcriptional activation, J. Control. Release 112 (2006) 382–388.
[3] D.G. Miller, P.R. Wang, L.M. Petek, R.K. Hirata, M.S. Sands, D.W. Russell, Gene targeting in vivo by adeno-associated virus vectors, Nat. Biotechnol. 24 (2006) 1022–1026.
[4] K. Itaka, K. Yamauchi, A. Harada, K. Nakamura, H. Kawaguchi, K. Kataoka, Polyion complex micelles from plasmid DNA and poly(ethylene glycol)-poly(L-lysine) block copolymer as serum-tolerable polyplex system: physicochemical properties of micelles relevant to gene transfection efficiency, Biomaterials 24 (2003) 4495–4506.
[5] A. Kim, E.H. Lee, S.H. Choi, C.K. Kim, In vitro and in vivo transfection efficiency of a novel ultradeformable cationic liposome, Biomaterials 25 (2004) 305–313.
[6] S.M. Kwon, H.Y. Nam, T. Nam, K. Park, S. Lee, K. Kim, I.C. Kwon, J. Kim, D. Kang, J.H. Park, S.Y. Jeong, In vivo time-dependent gene expression of cationic lipid-based emulsion as a stable and biocompatible non-viral gene carrier, J. Control. Release 128 (2008) 89–97.
[7] S. Hama, H. Akita, R. Ito, H. Mizuguchi, T. Hayakawa, H. Harashima, Quantitative comparison of intracellular trafficking and nuclear transcription between adenoviral and lipoplex systems, Mol. Ther. 13 (2006) 786–794.
[8] S. Hama, H. Akita, S. Iida, H. Mizuguchi, H. Harashima, Quantitative and mechanism-based investigation of post-nuclear delivery events between adenovirus and lipoplex, Nucleic Acids Res. 35 (2007) 1533–1543.